HOLOGRAPHIC INTERFEROMETRY MEASUREMENTS

OF SUBSONIC TURBULENT BOUNDARY LAYERS

D. W. Sinclair

ARO, Inc., a Sverdrup Corporation Company

PROPULSION WIND TUNNEL FACILITY
ARNOLD ENGINEERING DEVELOPMENT CENTER
AIR FORCE SYSTEMS COMMAND
ARNOLD AIR FORCE STATION, TENNESSEE 37389

February 1979

Final Report for Period October 1976 — September 1977

Approved for public release; distribution unlimited.

Prepared for

ARNOLD ENGINEERING DEVELOPMENT CENTER/DOTR
ARNOLD AIR FORCE STATION, TENNESSEE 37389

This report has been reviewed by the Information Office (OI) and is releasable to the National Technical Information Service (NTIS). At NTIS, it will be available to the general public, including foreign nations.

APPROVAL STATEMENT

This report has been reviewed and approved.

STANISLAUS L. LUDWIG, Captain (CF)
Project Manager, Research Division
Directorate of Test Engineering

Approved for publication:

FOR THE COMMANDER

ROBERT W. CROSSLEY, Lt Colonel, USAF
Acting Director of Test Engineering
Deputy for Operations

REPORT DOCUMENTATION PAGE		READ INSTRUCTIONS BEFORE COMPLETING FORM
1 REPORT NUMBER AEDC-TR-78-62	2 GOVT ACCESSION NO.	3 RECIPIENT'S CATALOG NUMBER
4 TITLE (and Subtitle) HOLOGRAPHIC INTERFEROMETRY MEASUREMENTS OF SUBSONIC TURBULENT BOUNDARY LAYERS		5 TYPE OF REPORT & PERIOD COVERED Final Report – October 1976 – September 1977
		6 PERFORMING ORG REPORT NUMBER
7 AUTHOR(s) D. W. Sinclair, ARO, Inc., a Sverdrup Corporation Company		8 CONTRACT OR GRANT NUMBER(s)
9 PERFORMING ORGANIZATION NAME AND ADDRESS Arnold Engineering Development Center/DOTR Air Force Systems Command Arnold Air Force Station, Tennessee 37389		10 PROGRAM ELEMENT PROJECT, TASK AREA & WORK UNIT NUMBERS Program Element 65807F
11 CONTROLLING OFFICE NAME AND ADDRESS Arnold Engineering Development Center/OIS Arnold Air Force Station, Tennessee 37389		12 REPORT DATE February 1979
		13 NUMBER OF PAGES 54
14 MONITORING AGENCY NAME & ADDRESS(If different from Controlling Office)		15 SECURITY CLASS (of this report) UNCLASSIFIED
		15a DECLASSIFICATION DOWNGRADING SCHEDULE N/A

16 DISTRIBUTION STATEMENT (of this Report)

Approved for public release; distribution unlimited.

17 DISTRIBUTION STATEMENT (of the abstract entered in Block 20, If different from Report)

18 SUPPLEMENTARY NOTES

Available in DDC

19 KEY WORDS (Continue on reverse side If necessary and identify by block number)

holographic	turbulent boundary layers
interferometry	Mach numbers
measurement	density
subsonic flow	profiles

20 ABSTRACT (Continue on reverse side If necessary and identify by block number)

Laser holographic interferometry was applied to the measure-
ment of density profiles of two-dimensional planar turbulent
boundary layers on the wall of the Acoustic Research Tunnel (ART)
at the Arnold Engineering Development Center (AEDC). Holograms
were produced at Mach numbers 0.50 and 0.65 by the finite fringe,
single-plate, dual-exposure method. The reconstructed image from
this type of hologram contains fringes that are shifted relative

DD FORM 1473 EDITION OF 1 NOV 65 IS OBSOLETE
1 JAN 73

20. ABSTRACT (Continued)

to a reference fringe by an amount that is proportional to the
difference in the densities at the two points. Therefore, it was
possible to determine the density profiles by measuring the
fringe shifts appearing in the reconstructed images. By assuming
adiabatic wall conditions, constant static pressure through the
boundary layer and a velocity-temperature relationship, it was
possible to use the density profiles to calculate velocity
profiles and to determine boundary-layer displacement thickness,
δ^*, momentum thickness, θ, shape factor, H, and skin friction, c_f.
The results of two velocity-temperature relations are presented,
and compared to data obtained by pitot, hot-wire, and split-film
probes. A description of the experimental facility, hardware for
data acquisition, data reduction methods, and a discussion of the
problems encountered in the holographic interferometry technique
are presented.

AFSC
Arnold AFS Tenn

PREFACE

CONTENTS

ILLUSTRATIONS

APPENDIX

1.0 INTRODUCTION

There has been a great deal of interest in recent years in the development and application of flow diagnostic techniques that are nondisturbing to the flow field. One such technique is laser holographic interferometry.

Much effort has been given to applying holographic interferometry to measurements in supersonic flow such as the work of Radley and Havener (Refs. 1 through 4), Zien and Ragsdale (Ref. 5), and Trolinger and O'Hare (Ref. 6). Kosakoski and Collins (Ref. 7) have used the dual-exposure holographic technique to make density measurements in transonic corner flow, but the application of holographic interferometry to subsonic flow has been almost totally neglected. The reason for this may be that density gradients in subsonic flow are much smaller than in supersonic flow. However, techniques such as fringe control exist which enable accurate measurements of small changes in density. By applying the finite fringe technique to subsonic flow, it is possible to make boundary-layer measurements without disturbing the flow. In addition, the holographic interferometry technique captures the entire flow field instantaneously; therefore, data acquisition time can be greatly reduced.

The purpose of this study was to determine if useful quantitative information could be extracted from holographic interferograms for flows with small gradients in density ($\leq$ 5 percent). For the study, the laser holographic interferometry technique was applied to the measurement of density profiles of two-dimensional, planar, turbulent boundary layers on the impermeable wall of the Acoustic Research Tunnel (ART) in the Propulsion Wind Tunnel Facility (PWT) of the Arnold Engineering Development Center (AEDC). Finite fringe, single-plate, dual-exposure holograms were produced at Mach numbers 0.50 and 0.65. The images recorded in the hologram were reconstructed, and experimental data in the form of fringe shifts were obtained. The measured fringe shifts

5

were used to calculate density profiles. By assuming adiabatic wall conditions, constant static pressure through the boundary layer, and a velocity-temperature relationship, it was possible to use the density profiles to calculate velocity profiles and subsequently determine boundary-layer displacement thickness, δ^*, momentum thickness, θ, shape factor, H, and skin friction, c_f. These quantities were compared with data obtained by pitot, hot-wire, and split-film probes.

A description of the experimental facility and apparatus is given and the data reduction equations are developed. Finally, recommendations are made for the further improvement of the holographic interferometry data reduction technique described in this report.

2.0 DESCRIPTION OF EXPERIMENTAL FACILITY AND APPARATUS

2.1 ACOUSTIC RESEARCH TUNNEL

The ART is an open circuit, atmospheric inbleed tunnel (see Fig. 1) that operates on the Plenum Evacuation System (PES) of the PWT Tunnel 16T. The ART was originally designed to study the acoustic characteristics of walls used in transonic wind tunnels and, as a result, the ART has a low background noise level as can be seen in Fig. 2. Figure 2 shows that the wall static pressure fluctuations are approximately 0.45 percent of the dynamic pressure over the entire Mach number range for the solid test section walls.

The demonstrated Mach number range of the ART is from 0.05 to 1.10 when ventilated walls and test section wall divergence are used. However, the use of solid walls and constant area test section limits the upper end of the Mach number range to 0.85 for the standard tunnel configuration shown in Fig. 1. The standard configuration consists of a converging nozzle with a contraction ratio of 16, a 6-in.-square test section that is 24 in. long and a 5-deg diffuser. The test section is

enclosed by a plenum as shown in Fig. 3. Also, Fig. 3 shows the axial location of the 8-in.-diam optical quality windows which provide visual access to the test section. Further details concerning the ART can be found in Ref. 8.

Two modifications were made to the standard configuration for this investigation. The first modification was the addition of a boundary-layer trip in the nozzle to fix the location of transition from a laminar to a turbulent boundary layer. The trip was fabricated from a 1/4-in.-wide strip of 0.004-in.-thick brass shim stock that was long enough to span the tunnel at the location shown in Fig. 1. The trip consisted of a series of hemispherical bumps 0.025 in. high and spaced 0.10 in. apart. The other modification was the addition of a 24-in.-long channel between the nozzle and the standard test section. With the boundary-layer channel in place, the distance between the trip and the measurement location was 54 in. The channel increases the boundary-layer thickness by a factor of two over that for the standard configuration and results in lowering the maximum Mach number to 0.78 when undiverged impermeable walls are used.
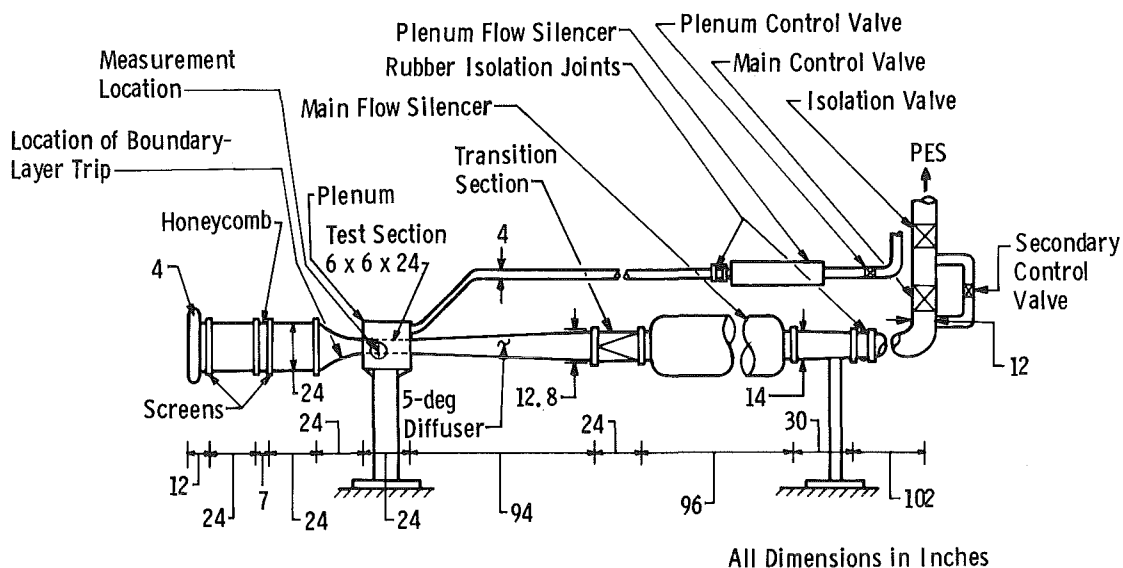
Figure 1. Schematic of Acoustic Research Tunnel.
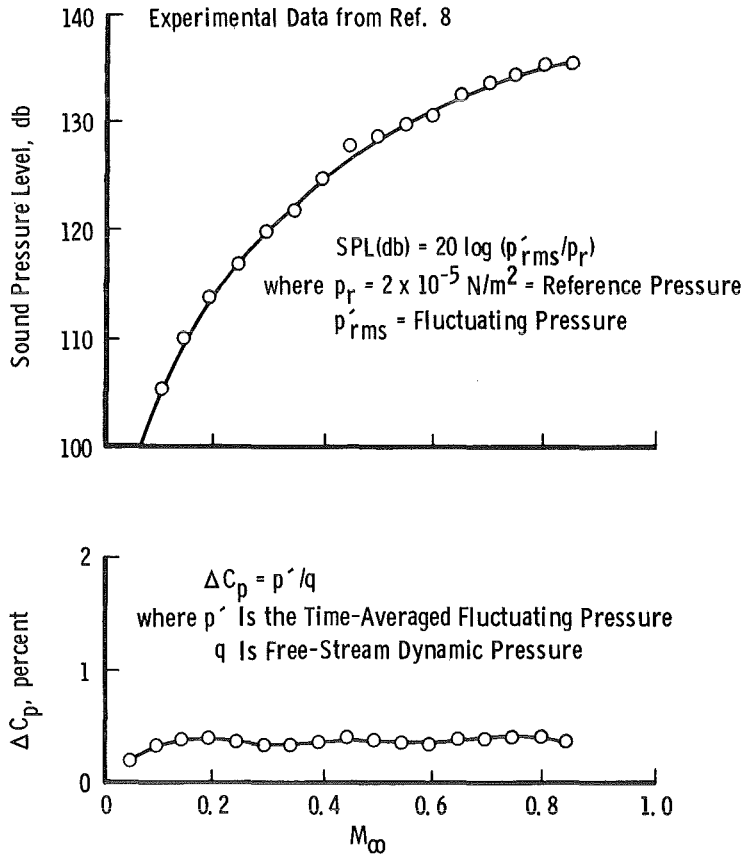
Figure 2. Noise levels in Acoustic Research Tunnel for solid
test section walls.
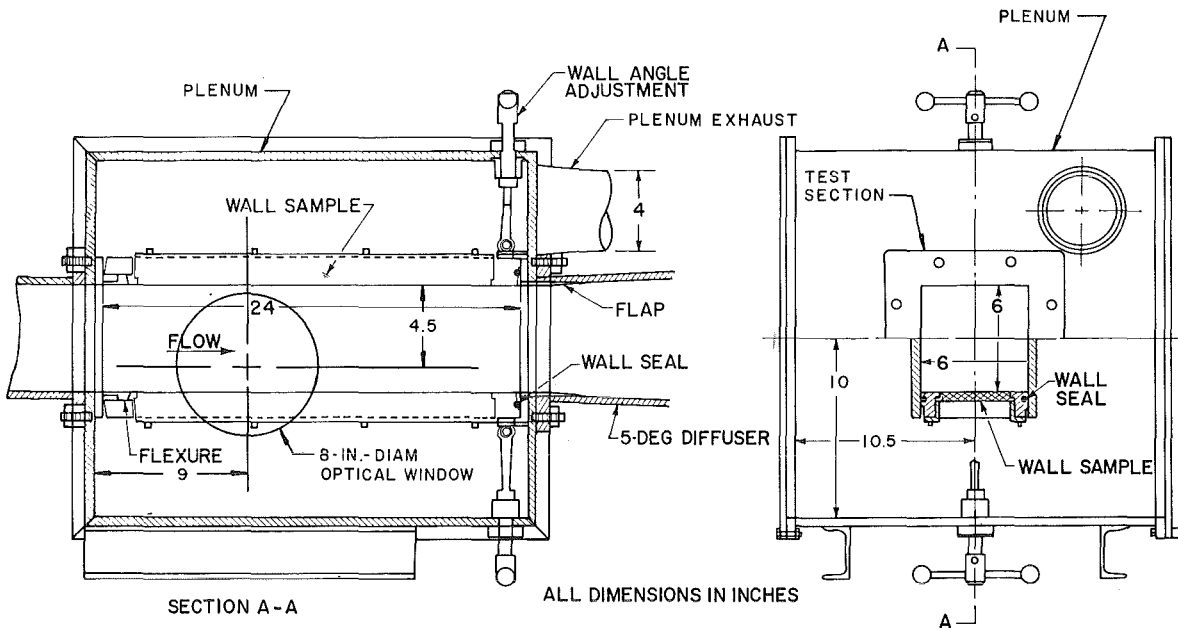
Figure 3. Schematic of test section and plenum of Acoustic Research Tunnel.

2.2 PROBE TRAVERSING MECHANISM

The probes used during this study were mounted on a traversing mechanism (see Fig. 4) that was located in a position that allowed the probes to be viewed through the test section window (see Fig. 5). This arrangement assured that the interferometer and probe data were for a boundary layer at approximately the same axial location in the tunnel.

The traversing mechanism was designed and found to provide probe positioning accuracies to within 0.003 in. The drive mechanism was equipped with antibacklash gears and a magnetic brake to avoid coasting at the end of movement. A linear potentiometer, mounted on the traversing strut, was used to indicate the probe position by means of a voltage output. Before each test, a calibration of the traversing mechanism was performed so that the distance from the probe to the wall could be read directly on a Fluke® Model 8400 digital voltmeter.
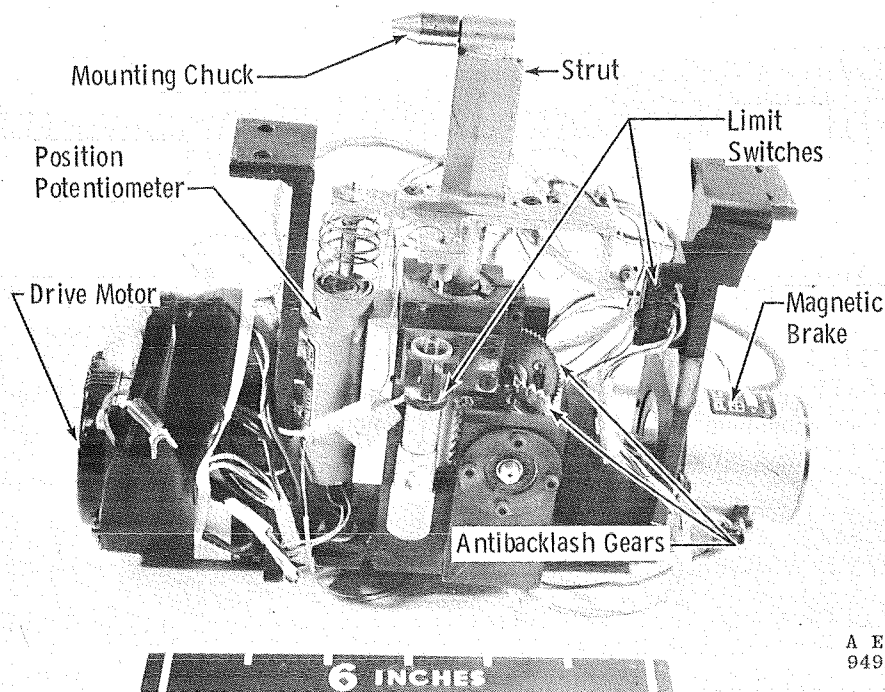
Figure 4. Photograph of probe traversing mechanism.
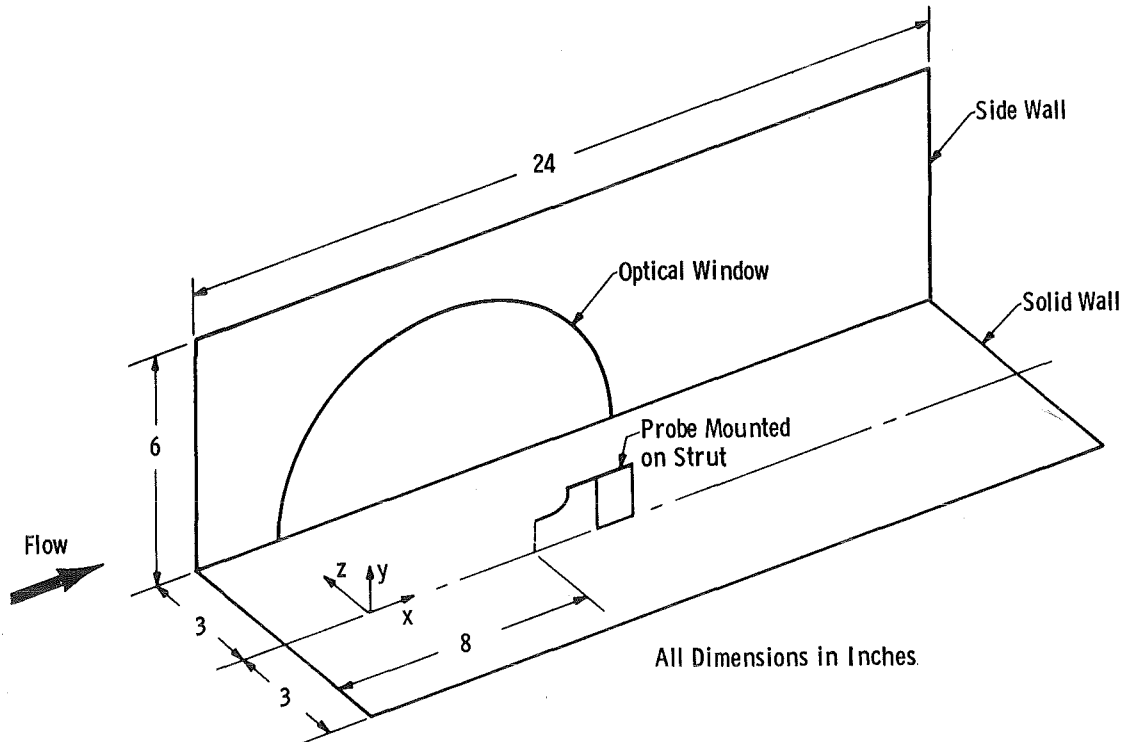
Figure 5. Location of probe in test section.

2.3 PROBES

2.3.1 Pitot Probe

The pitot probe used in this study was constructed from a seamless stainless steel tube with an outside diameter of 0.065 in. The end of the tube was flattened and shaped to form an opening that was approximately 0.002 in. in height and 0.1 in. in width. The overall height of the probe at the tip was approximately 0.005 in. with a tubing wall thickness of approximately 0.0015 in. This shape is often used in boundary-layer work to provide greater profile resolution and minimize pressure lag. The probe was mounted as shown in Fig. 6, and connected to a Kistler® Series 314 (0 to 15 psi) pressure transducer. The transducer was calibrated to read pressure in pounds per square foot directly on a Fluke Model 8400 digital voltmeter.
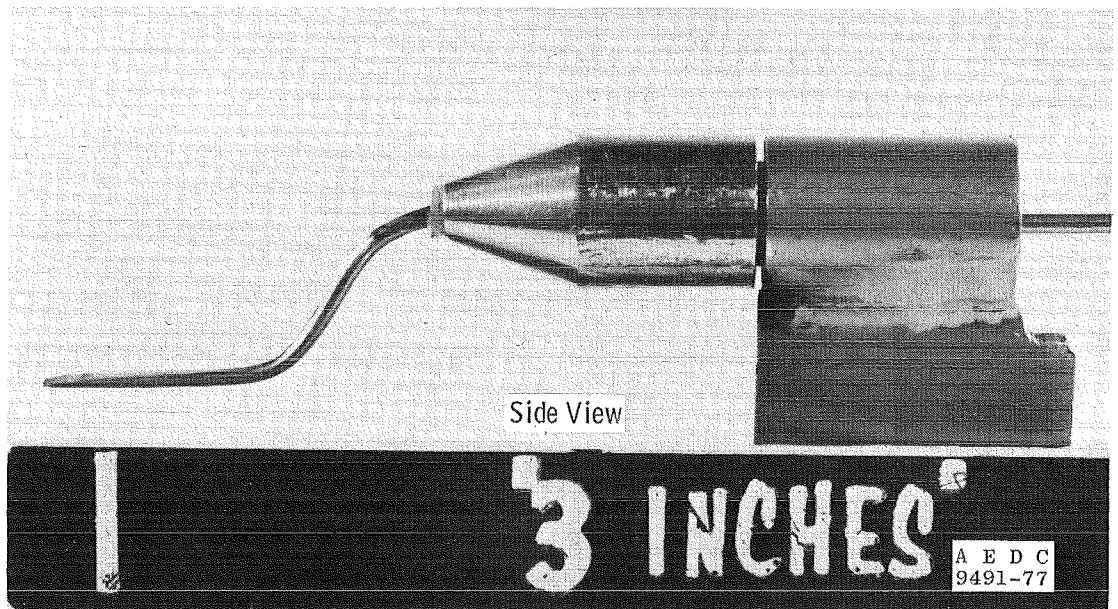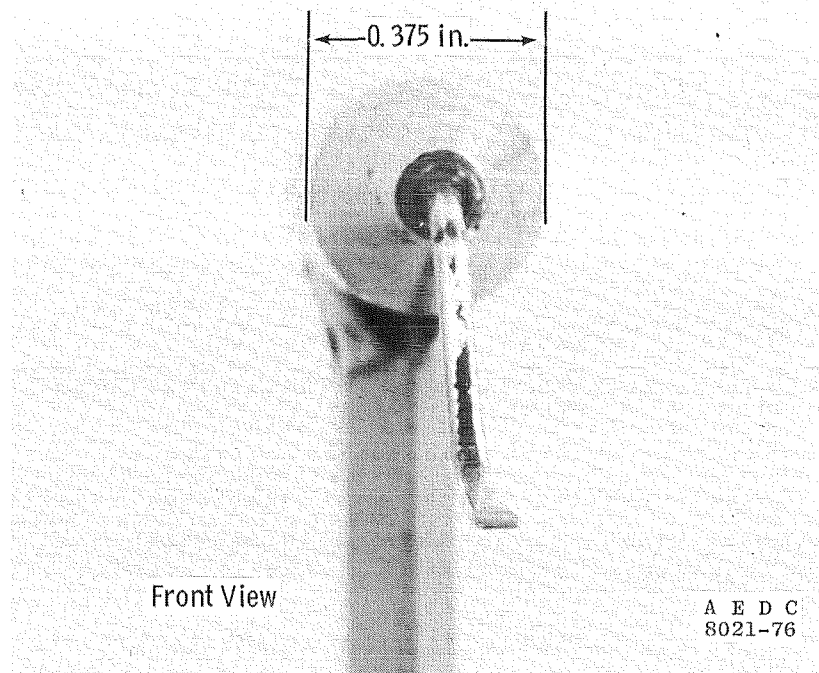
Figure 6. Front and side view of pitot probe.

2.3.2 Hot-Wire Probe

The hot-wire probe (see Fig. 7) was a Thermo Systems[®] Model 1248, x-shaped, cylindrical film with a wire diameter of 0.001 in. and a sensing length of 0.08 in. The output from the hot-wire probe was
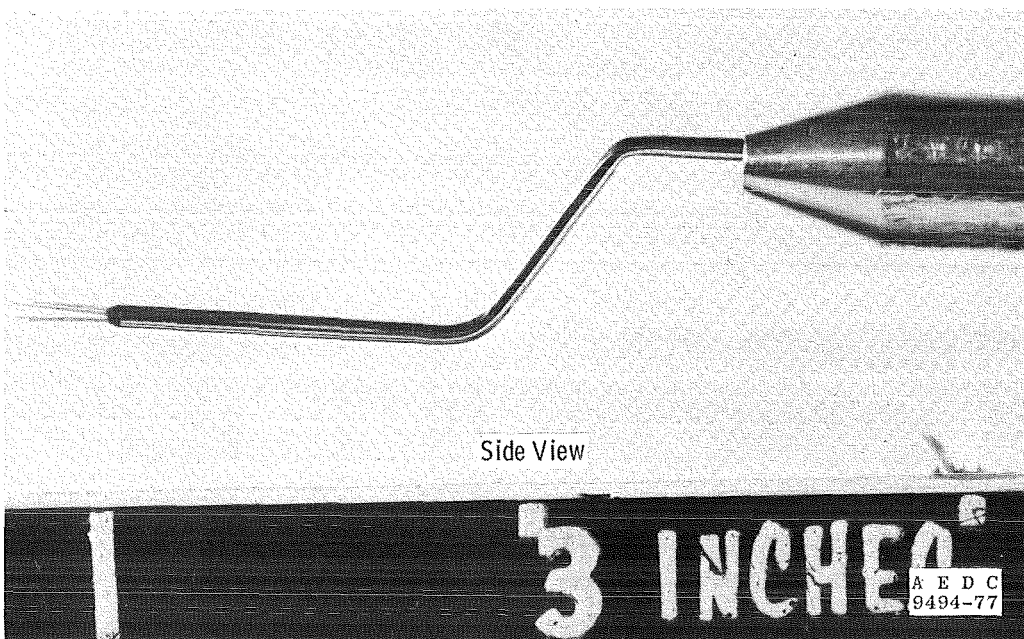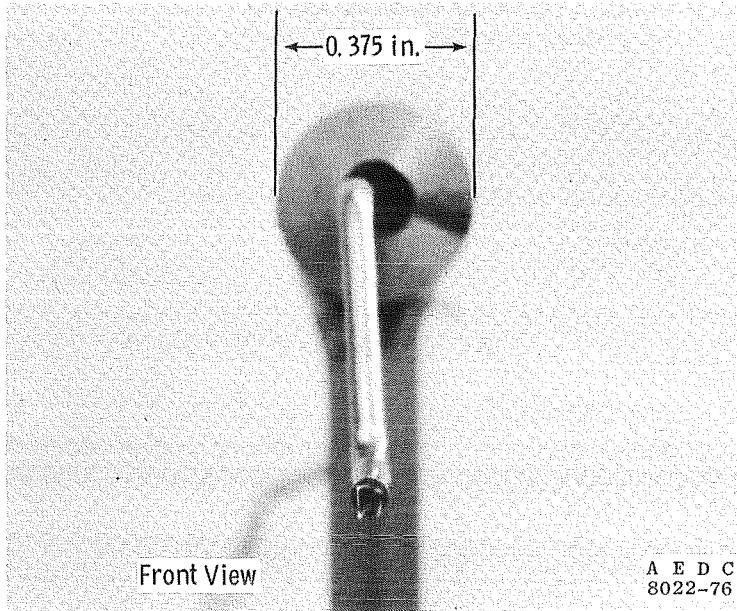
Figure 7. Front and side view of hot-wire probe.

electronically processed and the final result appeared as a voltage reading on a Fluke Model 8400 digital voltmeter. The hot-wire probe was capable of measuring two components of velocity as well as their fluctuations. However, only the mean velocities in the axial direction are reported here.

2.3.3 Split-Film Probe

The split-film probe used in this study (see Fig. 8) was a Thermo Systems Model 1288 with a ceramic center and thin aluminum coating. The sensing element on this probe was 0.006 in. in diameter and had a sensing length of 0.08 in. The voltage output from the split-film probe was read on a Fluke Model 8400 digital voltmeter. Like the hot wire, the split film was capable of measuring two components of mean and fluctuating velocity, but only the mean velocities in the axial direction are reported here.

2.4 HOLOGRAPHIC INTERFEROMETER

A schematic of the holographic interferometer used in this study is presented in Fig. 9. The interferometer utilized a Korad Model K1Q pulsed ruby laser. The laser beam was spatially filtered and split into two beams of approximately equal intensity. The object beam was expanded and passed through the ART test section. The reference beam was directed over the test section and reunited with the object beam at the photographic plate. This particular arrangement is a slightly modified Mach-Zehnder Interferometer (see Fig. 10). If Figs. 9 and 10 are compared, one can see a difference in that the object and reference beams of the Mach-Zehnder Interferometer are rejoined at a second semireflecting mirror instead of at a photographic plate as in the holographic interferometer. Photographs of the actual components of the interferometer are shown in Fig. 11.
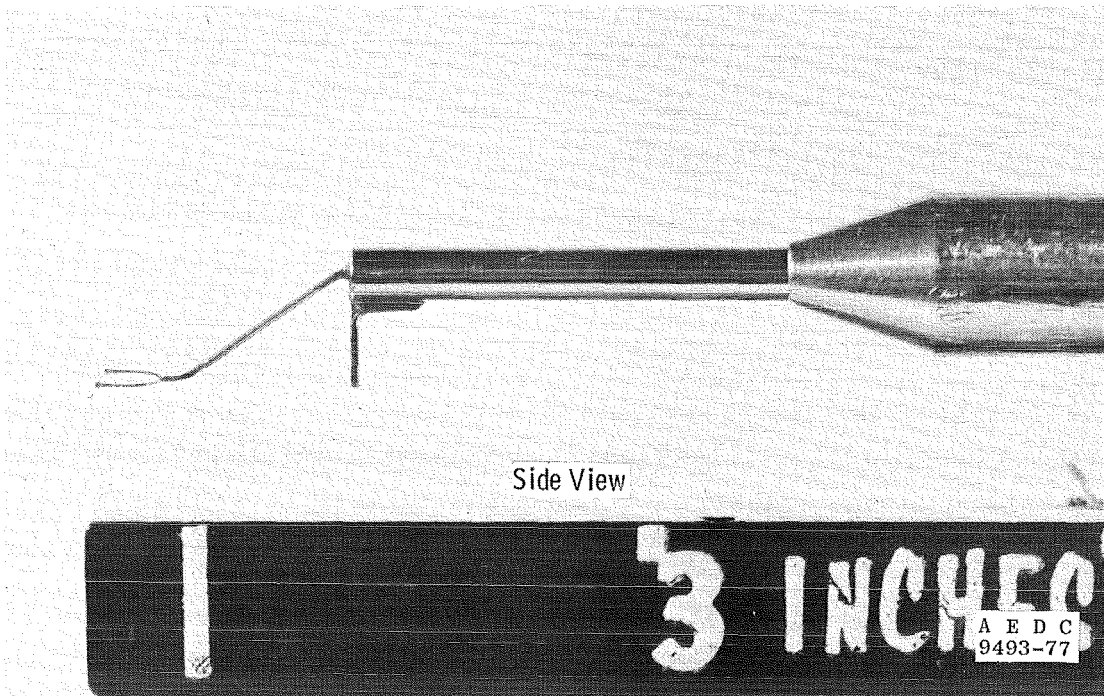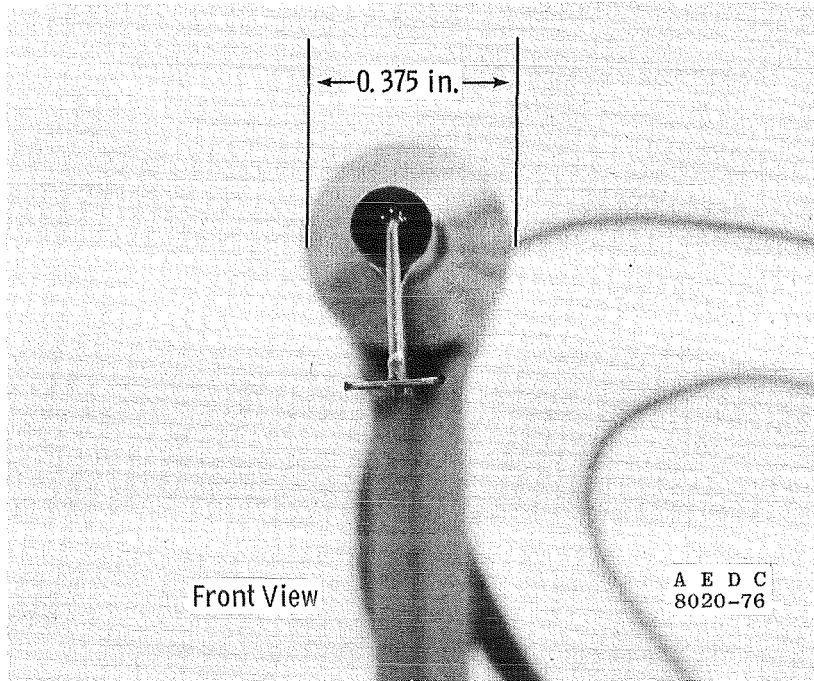
Figure 8. Front and side view of split-film probe.
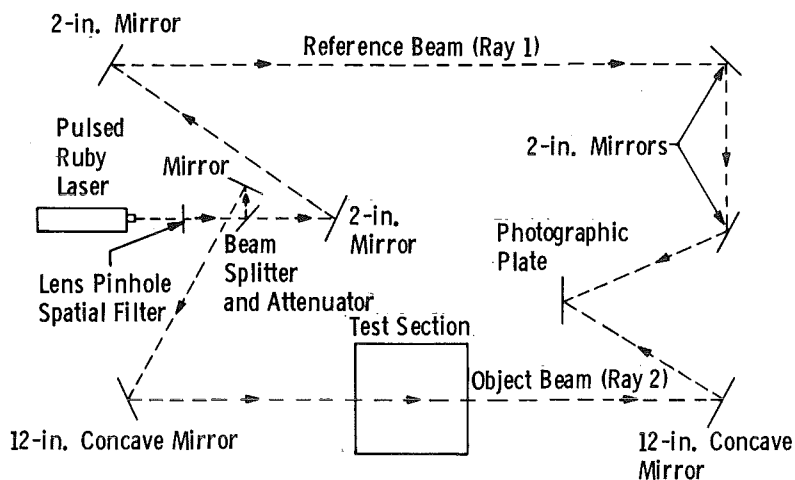
Figure 9. Schematic of Acoustic Research Tunnel holographic
interferometry system.
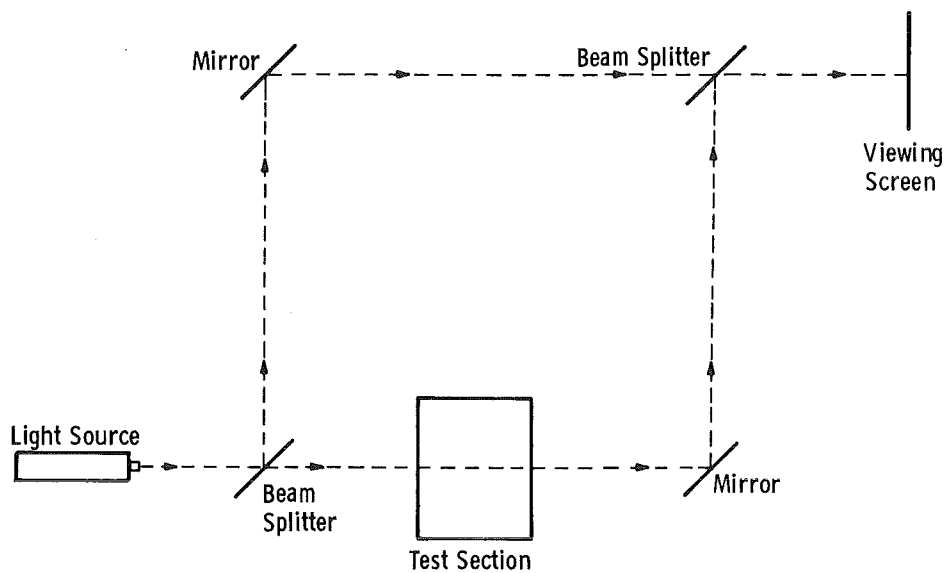
Figure 10. Schematic of Mach-Zehnder Interferometer.
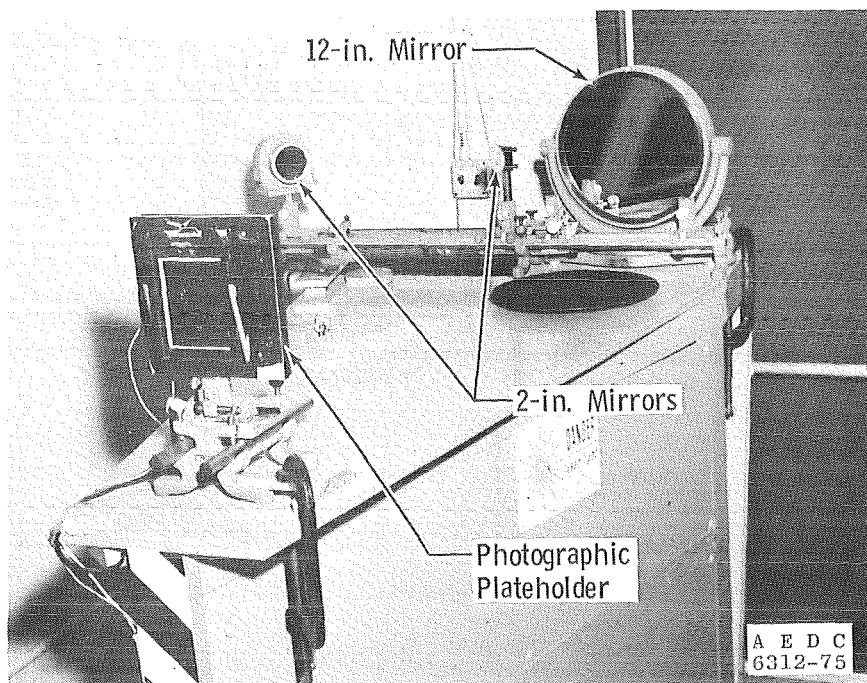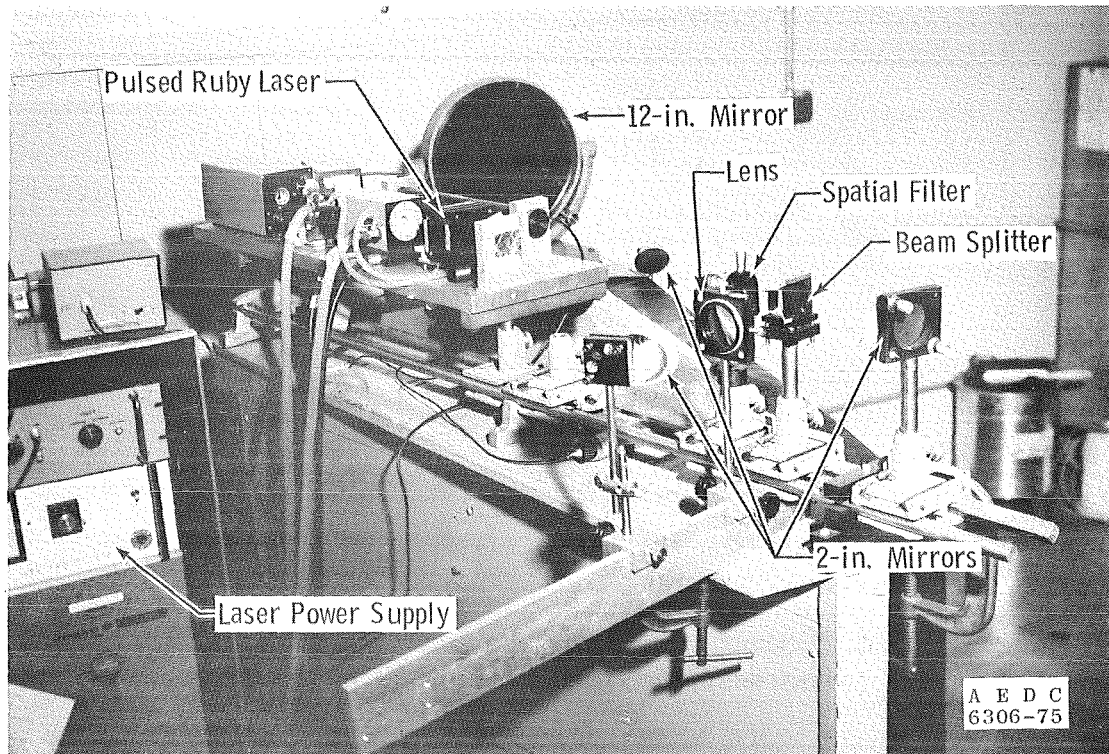
Figure 11. Photographs of Acoustic Research Tunnel holographic interferometry system.

3.0 EXPERIMENTAL PROCEDURE

For each experiment in this study, boundary-layer data were obtained simultaneously by probe and holographic interferometry techniques. Before each run, a probe was selected and mounted in the tunnel as shown in Fig. 5. A calibration of the probe position and test firings of the pulsed ruby laser were performed as part of the pretest procedures.

When tunnel flow conditions were established, probe data were taken starting as close to the wall as practical without causing damage to the probe. This exercise in caution was especially important when the hot-wire and split-film probes were used. From the starting position, the probe was moved in small increments outward from the wall until free-stream conditions were reached (i.e., the boundary-layer edge location and free-stream conditions were defined when the probe readings remained essentially constant over several probe movements). At each probe location, the output signal from the probe was time averaged for two to five minutes, and the average value was recorded along with probe position. The time required to obtain data in this manner was between one to three hours per profile depending on the probe used.

During the process of making probe measurements, several holograms were produced. The technique used in producing the holograms was the finite fringe, single-plate, dual-exposure method. In this method, the same photographic plate is exposed at two different times. Between exposures, the photographic plate is translated to provide control of the fringes that appear in the reconstructed image of the hologram. The procedure chosen for this study was to expose the photographic plate without flow in the test section, translate the plate 1 mm along the axis of the tunnel, and expose the plate a second time with flow in the test section at the desired flow condition. The 1-mm movement was determined experimentally as the distance that gave the easiest fringe pattern to interpret on the equipment that was available for data analysis.

3.1 PROBE CALIBRATION

3.1.1 Probe Position Calibration

The method of calibrating the linear potentiometer used to indicate probe position was the same for all three probes. A two-point calibration was sufficient because of the high linearity and repeatability of the potentiometer. The two reference distances chosen for the calibration were the wall and the top of a 0.5-in. precision-machined block. The 0.5-in. reference distance was chosen because the boundary layers to be measured were expected to be of comparable thickness. However, the high linearity of the potentiometer allowed measurements to be made beyond the 0.5-in. calibration point with no loss in accuracy.

During calibration, the tip of the probe was visually aligned with the reference points, and the output of the potentiometer circuit was adjusted to give a reading of 0.000 volts with the probe at the wall and 0.500 volts with the probe tip even with the top of the machined block. Therefore, the distance from the probe to the wall could be read directly on the digital voltmeter.

3.1.2 Probe Output Calibration

3.1.2.1 Pitot Probe

The total pressure measured by the pitot probe was converted to a direct-current electrical signal by a Kistler Series 314 pressure transducer. The transducer was calibrated over the range from 0 to 2,000 pounds per square foot before each run. The zero point was established by venting both sides of the transducer to the atmosphere. Several calibration points were set within the span of the transducer by applying a known pressure to the pressure side while the reference side was exposed to a vacuum.

18

3.1.2.2 Hot-Wire and Split-Film Probes

The procedures for calibrating the hot-wire and split-film probes were similar in nature. The calibrations were performed on a Thermo Systems Model 1125 calibrator as outlined by the manufacturer. The calibration procedure consisted of mounting the probe in the calibrator and directing a jet of known mass flow rate over the probe. A calibration curve was generated by varying the mass flow rate and recording the output from the probe.

3.2 PROBE DATA REDUCTION

The data obtained by probe measurements were input into a pitot data reduction program developed by Whitfield (Ref. 9) which was modified by Benek (Ref. 10) to accept hot-wire and split-film data. Pitot data input to this program were in the form of local total-pressure ratio, P_T/P_{T_∞}, as a function of distance from the wall, Y. The hot-wire and split-film data were reduced to local velocity ratios, u/u_∞, by methods similar to those presented by Spencer and Jones (Ref. 11) and Sanborn and Seegmiller (Ref. 12), respectively. These values of local velocity ratio were then input into the data reduction program as a function of distance from the wall, Y. In addition to the probe data, the data reduction program required the tunnel total temperature, total pressure, and free-stream Mach number.

The measured total-pressure ratio, P_T/P_{T_∞}, was used to determine the local Mach number ratio, M/M_∞. The definition of Mach number was employed to obtain the relation

$$\frac{M}{M_\infty} = \frac{u}{u_\infty} \left(\frac{T_\infty}{T} \right)^{\frac{1}{2}} \tag{1}$$

19

The Crocco-type relation for nonunity Prandtl number and adiabatic wall condition developed by Whitfield and High (Ref. 13) was used as a second equation for the unknowns u/u_∞ and T/T_∞. The relation is given as

$$\frac{T}{T_\infty} = 1 + \frac{\gamma-1}{2} M_\infty^2 \left[1 - \left(\frac{u}{u_\infty}\right)^2 \right] + (1 - Pr_m) \left\{ \frac{K(\gamma-1)M_\infty^2}{(a+1)(a-1)} \right.$$

$$\left. \left[1 - \left(\frac{u}{u_\infty}\right)^{a+2} \right] + \frac{(\gamma-1)}{2} M_\infty^2 \left[1 - \left(\frac{u}{u_\infty}\right)^2 \right] + f(1) - f\left(\frac{u}{u_\infty}\right) \right\} \quad (2)$$

where

$$f\left(\frac{u}{u_\infty}\right) = \frac{\Delta}{(\gamma-1)M_\infty^2} \left[(\zeta - \Delta)\ln|\zeta - \Delta| - (\zeta + \Delta)\ln|\zeta + \Delta| \right]$$

$$\zeta = -(\gamma - 1) M_\infty^2 \frac{u}{u_\infty}$$

$$\Delta = \left[2(\gamma - 1) M_\infty^2 \left(1 + \frac{\gamma-1}{2} M_\infty^2 \right) \right]^{\frac{1}{2}}$$

$$K = 10m$$

$$a = 2.5m$$

$$m = 7$$

and Pr_m is the van Driest mixed Prandtl number composed of the laminar and turbulent contributions to viscosity and thermal conductivity. Equations (1) and (2) were solved simultaneously by Newton-Raphson iteration to obtain local values of velocity ratio, u/u_∞, and temperature ratio, T/T_∞.

The hot-wire and split-film data input in the form of velocity ratio, u/u_∞, as a function of Y were substituted directly into Eq. (2) to calculate the local temperature ratio, T/T_∞.

Once the values u/u_∞ and T/T_∞ were found, the data reduction proceeded in the same manner for each type of probe. First, displacement thickness, δ^*, was calculated using the definition

$$\delta^* = \int_0^{Y_\infty} \left(1 - \frac{\rho u}{\rho_\infty u_\infty} \right) dy \tag{3}$$

The density ratio, ρ/ρ_∞, was found by assuming constant pressure through the boundary layer so that

$$\frac{\rho}{\rho_\infty} = \frac{T_\infty}{T}$$

Then, momentum thickness, θ, was determined by

$$\theta = \int_0^{Y_\infty} \frac{\rho u}{\rho_\infty u_\infty} \left(1 - \frac{u}{u_\infty} \right) dy \tag{4}$$

Shape factor, H, was calculated by

$$H = \frac{\delta^*}{\theta} \tag{5}$$

and, finally, the value of skin friction, c_f, associated with the measured profile was found by fitting the data to the compressible law of the wall as formulated by Fenter and Stalmach (Ref. 14)

$$\frac{\sin^{-1} \left(\sigma^{\frac{1}{2}} \frac{u}{u_\infty} \right)}{\left(\sigma \frac{c_f}{2} \frac{T_w}{T_\infty} \right)^{\frac{1}{2}}} = 5.75 \, \log_{10} \left[Re_{\infty,y} \frac{\mu_\infty}{\mu_w} \left(\frac{c_f}{2} \frac{T_\infty}{T_w} \right) \right]^{\frac{1}{2}} + 5.1$$

where

$$\sigma = \frac{(\gamma-1)}{2} M_\infty^2 \left/ \left(1 + \frac{\gamma-1}{2} M_\infty^2 \right) \right.$$

$$\frac{T_w}{T_\infty} = 1 + r \frac{\gamma-1}{2} M_\infty^2$$

$$r = 0.88$$

μ is the laminar viscosity

The calculated values of δ^*, θ, and H were corrected within the program by the Wall-Overlap Layer (WOLL) model described in Ref. 10. The WOLL model and the value of c_f were used to supply additional points to the profile close to the wall where data are difficult to obtain by probe measurements.

4.0 HOLOGRAPHIC INTERFEROMETRY DATA ANALYSIS

Holographic interferometry is an optical technique that gives a direct indication of relative density. The principle involved is that light travels at different speeds through media of different densities. By referring to Fig. 9, it is possible to explain how this principle is applied. The figure shows that the beam from the laser is divided into two beams of approximately equal intensity. One beam (object beam) passes through the test section while the other (reference beam) does not. If the optical path length that each of these beams travels is the same, then the beams arriving at the photographic plate will be in phase. Now, if the density in the test section is changed, the optical path length will also be changed, and the two beams will not be in phase when they arrive at the photographic plate. The effect is the appearance of light and dark areas called fringes. These fringes represent rays of light that travel optical paths of equal length or paths that differ by some integer multiple of the wavelength of the laser beam. Therefore, if the density is known in the test section at some point, the density at other points can be determined by methods that will be discussed in the next section.

4.1 DENSITY-FRINGE SHIFT RELATION

A hologram is a diffracting record of the interference of a particular object (the density field) and a particular reference beam. The method for determining the density field depends on the technique used in producing the hologram. The two types of holograms considered were

the infinite fringe and the finite fringe holographic interferogram. An
example of an interferogram produced by each method is given in Fig. 12.
Both methods require two exposures of the photographic plate, one with
no flow in the test section and one with flow. The difference in the
two methods is that between exposures the photographic plate is translated
to a new position in the finite fringe method and is held fixed in the
infinite fringe method.
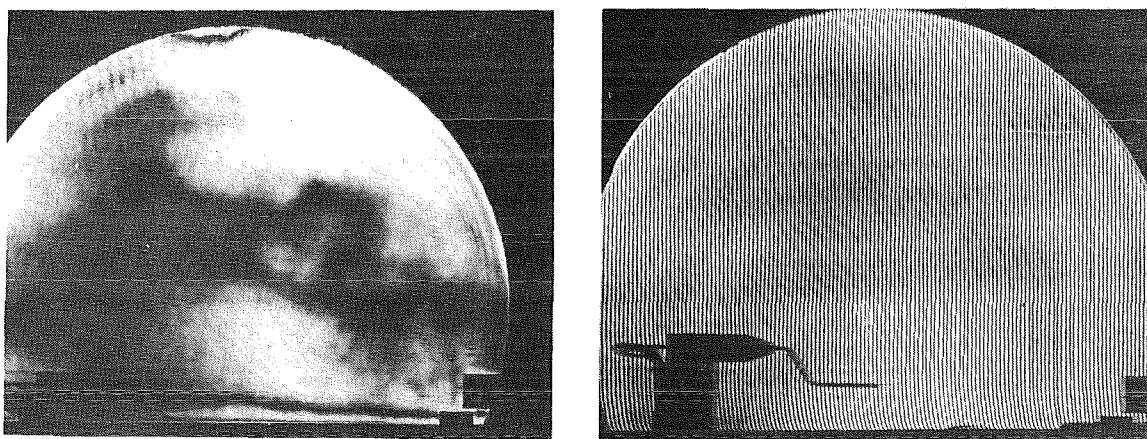
a. Infinite fringe (M∞ = 0.50)   b. Finite fringe (M∞ = 0.50)

Figure 12. Examples of infinite and finite fringe holographic interferograms.

The fringes that appear in the infinite fringe interferogram represent
contours of constant density in the flow field. The fringes are formed
by the difference in phase of the light in the adjacent fringes. The
phase difference between adjacent dark or light fringes is equal to one
wavelength of the incident light. Therefore, to obtain data from the
infinite fringe interferogram, it is necessary to determine the amount
of density change that will produce a change in optical path length
equal to one wavelength of the laser light source. Then, by counting
the number of fringes between a known reference density and the point of
interest, the density at that point can be determined. The major drawback
of this method is that the smallest unit of density change that can be

measured is the change in density that produces a phase difference of one-half wavelength (i.e. the difference between a dark and adjacent light fringe). This makes the infinite fringe technique attractive in flows with large density gradients. However, in flows with small density gradients, an insufficient number of fringes is produced to provide the resolution necessary to derive information about the boundary layer (see Fig. 12a).

For greater resolution in flows with small density gradients, the number of fringes in the flow field is controlled by adjusting the geometry of the optical system, in this case by translating the photographic plate between exposures. If the density in the test section is the same during both exposures of the photographic plate, then a series of uniformly spaced parallel fringes that are perpendicular to the line of plate movement will appear in the interferogram. If there is a difference in density between exposures, the fringes will remain uniformly spaced, but will be shifted in the direction parallel to the plate movement (see Fig. 12b). The fringe shift is a measure of the change in density in the test section. The shifted fringes appear as continuous lines on the reconstructed image of the hologram; therefore, many measurements of fringe shift can be made to provide greater resolution in the boundary layer. It was for this reason that the finite fringe technique was chosen in this study. Further details of the infinite and finite fringe techniques can be found in Ref. 15.

The method of calculating the density at various points in the flow field using the measured fringe shifts from the finite fringe holographic interferograms will now be discussed.

Because light travels at different speeds through media of different densities, one can calculate the time it takes a ray of light to traverse the width of the test section, L. The time, t, is given by

24

$$t = \int_0^L \frac{d\ell}{\nu}$$

where ν is the speed of light in the medium of interest. Using this expression, the difference between the time required for light to traverse the test section with and without flow is given by

$$\Delta t = t_2 - t_1 = \int_0^L \left[\frac{1}{\nu_2} - \frac{1}{\nu_1} \right] d\ell \tag{6}$$

where the subscripts 1 and 2 denote no flow and flow conditions, respectively.

Since the index of refraction, n, is defined as

$$n = \frac{c}{\nu}$$

where c is the speed of light in a vacuum, Eq. (6) can be rewritten as

$$\Delta t = \frac{1}{c} \int_0^L \left[n_2 - n_1 \right] d\ell$$

and the change in optical path length, Δx, (see Ref. 16) is given by

$$\Delta x = c \Delta t = \int_0^L \left[n_2 - n_1 \right] d\ell \tag{7}$$

In terms of data appearing on the interferogram, a change in optical path length by one wavelength, λ, of the incident light will be proportional to the distance between the centers of two adjacent fringes of the same type (i.e., light to light or dark to dark, see Figs. 12b and A-1). Therefore, one can define the change in optical path length in terms of the wavelength of the incident light, λ, the fringe spacing, θ, and the fringe shift, $\Delta\phi$, as

$$\Delta x = \frac{\Delta\phi}{\phi} \lambda \tag{8}$$

25

Substituting Eq. (8) into Eq. (7) gives

$$\frac{\Delta\phi}{\phi} \lambda = \int_0^L \left[n_2 - n_1 \right] d\ell \tag{9}$$

In gases, the speed of light is only slightly less than the speed of light in a vacuum. The difference is directly proportional to the density and is given to good accuracy by the Gladstone-Dale Equation (Ref. 16)

$$n = 1 + \beta \frac{\rho}{\rho_s} \tag{10}$$

where ρ_s is the reference density at standard conditions

ρ is the density of the gas at conditions other than standard

β is a constant for a particular gas, dependent on ρ_s

Substituting Eq. (10) into Eq. (9) gives

$$\frac{\Delta\phi}{\phi} \lambda = \frac{\beta}{\rho_s} \int_0^L \left[\rho_2 - \rho_1 \right] d\ell$$

Because the subscripts 1 and 2 refer to the no-flow and flow conditions, respectively, one can substitute the densities occurring in the tunnel under these conditions and rewrite the equation as

$$\frac{\Delta\phi}{\phi} \lambda = \frac{\beta}{\rho_s} \int_0^L \left[\rho - \rho_o \right] d\ell \quad , \tag{11}$$

where ρ_o is the density in the tunnel without flow and ρ is the local density with flow.

For this study, it was assumed that the boundary layer was two-dimensional (i.e., the density was uniform across the test section including the boundary layers on the sidewalls of the test section). Using this assumption, Eq. (11) can be integrated to yield

$$\rho - \rho_0 = \frac{\lambda \rho_s}{\beta L} \frac{\Delta \phi}{\phi} \qquad (12)$$

The nature of the fringe shifts involved is now examined.

In the study of boundary layers, it is of interest to relate the local flow conditions to the free-stream conditions. Equation (12) relates the local flow conditions to the total conditions; therefore, the fringe shifts will be with respect to these total conditions. In addition, the density in the plenum surrounding the test section changes between the no-flow and flow conditions, and a fringe shift will occur because of this effect. Therefore, the total fringe shift observed can be broken into three components such that

$$\Delta \phi = \Delta \phi_\infty + \Delta \phi_{local} + \Delta \phi_{plenum} \qquad (13)$$

where

$\Delta \phi_\infty$ is the fringe shift of the free stream measured relative to to the total density

$\Delta \phi_{local}$ is the fringe shift of the local density measured relative to the free-stream density

$\Delta \phi_{plenum}$ is the fringe shift attributed to the density change in the plenum measured relative to the free-stream density

Substituting Eq. (13) in Eq. (12) and solving for ρ/ρ_0 gives

$$\frac{\rho}{\rho_0} = 1 + \frac{\lambda}{\beta L} \frac{\rho_s}{\rho_0} \left[\frac{\Delta \phi_\infty + \Delta \phi_{local} + \Delta \phi_{plenum}}{\phi} \right] \qquad (14)$$

Evaluating Eq. (14) in the free stream gives

$$\frac{\rho_\infty}{\rho_0} = 1 + \frac{\lambda}{\beta L} \frac{\rho_s}{\rho_0} \left[\frac{\Delta \phi_\infty + \Delta \phi_{plenum}}{\phi} \right] \qquad (15)$$

27

Note that $\Delta\phi_{local}$ is zero at this point, because it is measured relative to the free stream.

Finally, subtracting Eq. (15) from Eq. (14) yields

$$\rho - \rho_\infty = \frac{\lambda \rho_s}{\beta L} \frac{\Delta\phi_{local}}{\phi} \qquad (16)$$

Equation (16) shows that if the fringe shifts are measured relative to the free stream, then the density measurements are independent of the fringe shift caused by the plenum. However, it should be mentioned that this is true only if the density in the plenum is constant and uniform. The effect is to shift each point in the fringe by an equal amount. The assumption of constant density in the plenum was assumed valid for the experiments conducted because there was no flow in the plenum (solid test section walls were used and there was no plenum suction). Equation (16) provides an expression which relates the local density to measurable quantities. The method used in reading fringe shifts from the holographic interferograms is presented in Appendix A. Next, the density measurements will be related to velocity by application of two different velocity-temperature relations.

4.2 VELOCITY-TEMPERATURE RELATIONS

The two velocity-temperature relationships considered during during this study were (1) the modified Crocco relation and (2) a relationship presented by Whitfield and High (Ref. 13) for a turbulent boundary layer with nonunity Prandtl number.

4.2.1 Modified Crocco Relation

The modified Crocco relation is given by

$$T = T_w + (T_{aw} - T_w) \frac{u}{u_\infty} - (T_{aw} - T_\infty) \left(\frac{u}{u_\infty}\right)^2 \qquad (17)$$

where the subscripts w, aw, and ∞ are for wall, adiabatic wall, and free-stream conditions, respectively.

Operation of the ART has shown that after a short run time (15 to 20 minutes), the walls have reached adiabatic conditions. Therefore,

$$T_w = T_{aw}$$

and Eq. (17) can be simplified to

$$T = T_{aw} - (T_{aw} - T_\infty) \left(\frac{u}{u_\infty}\right)^2$$

Dividing both sides of this equation by T_∞ yields

$$\frac{T}{T_\infty} = \frac{T_{aw}}{T_\infty} - \frac{T_{aw}}{T_\infty} - 1 \left(\frac{u}{u_\infty}\right)^2 \tag{18}$$

Because the static pressure is assumed constant through the boundary layer, application of the perfect gas law allows the temperature to be related to the density by

$$\frac{T}{T_\infty} = \frac{\rho_\infty}{\rho} \tag{19}$$

By substituting Eq. (19) into Eq. (18), recognizing that

$$\frac{T_{aw}}{T_\infty} = 1 + r \frac{\gamma - 1}{2} M_\infty^2$$

where r is the recovery factor, and solving for u/u_∞, yields

$$\frac{u}{u_\infty} = \left\{ 1 + \frac{1 - \frac{\rho_\infty}{\rho}}{r \frac{\gamma - 1}{2} M_\infty^2} \right\}^{\frac{1}{2}} \tag{20}$$

Equation (20) gives the ratio of the local to the free-stream velocity in terms of the ratio of the local to the free-stream density and other measurable quantities. By solving Eq. (16) for ρ/ρ_∞, one finds

$$\frac{\rho}{\rho_\infty} = 1 + S \frac{\Delta\phi_{local}}{\phi} \tag{21}$$

where

$$S = \frac{\lambda}{\beta L} \frac{\rho_s}{\rho_\infty}$$

Note that S is constant for a given flow condition, because the free-stream density, ρ_∞, will be fixed by the tunnel total temperature, total pressure, and the free-stream Mach number. Equation (21) can be substituted into Eq. (20) to yield

$$\frac{u}{u_\infty} = \left\{ 1 + \frac{S \frac{\Delta\phi_{local}}{\phi}}{\left(1 + S \frac{\Delta\phi_{local}}{\phi}\right)\left(r \frac{\gamma-1}{2} M_\infty^2\right)} \right\}^{\frac{1}{2}} \tag{22}$$

Equation (22) gives u/u_∞ in terms of the local fringe shift and other measurable quantities. Data reduction by Eq. (22) will be referred to as Method 1.

A much simpler approximation of Eq. (22) can be found by solving Eq. (16) for ρ_∞/ρ to obtain

$$\frac{\rho_\infty}{\rho} = 1 - S' \frac{\Delta\phi_{local}}{\phi} \tag{23}$$

where $S' = \frac{\lambda}{L\beta} \frac{\rho_s}{\rho}$. Note that S' is not a constant as in the previous method, because it contains the value of the local density at the point of measurement.

Evaluating Eq. (23) at the wall gives

$$\frac{\rho_\infty}{\rho_w} = 1 - \frac{\lambda}{L\beta} \frac{\rho_s}{\rho_w} \frac{\Delta\phi_w}{\phi} \tag{24}$$

Combining Eq. (23) and Eq. (24) yields

$$\frac{1 - \frac{\rho_\infty}{\rho}}{1 - \frac{\rho_\infty}{\rho_w}} = \frac{\rho_w}{\rho} \frac{\Delta\phi_{local}}{\Delta\phi_w} \tag{25}$$

Again, by applying the adiabatic wall condition and perfect gas law, one can write

$$\frac{\rho_\infty}{\rho_w} = \frac{T_{aw}}{T_\infty} = 1 + r\frac{\gamma-1}{2}M_\infty^2$$

Substituting into Eq. (25) yields

$$1 - \frac{\rho_\infty}{\rho} = -r\frac{\gamma-1}{2}M_\infty^2\frac{\rho_w}{\rho}\frac{\Delta\phi_{local}}{\Delta\phi_w}$$

and substituting this result into Eq. (20) gives

$$\frac{u}{u_\infty} = \left\{1 - \frac{\rho_w}{\rho}\frac{\Delta\phi_{local}}{\Delta\phi_w}\right\}^{\frac{1}{2}} \qquad (26)$$

The term ρ_w/ρ varies from 1.0 at the wall to $1.0/(1.0 + r\frac{\gamma-1}{2}M_\infty^2)$ in the free stream. For subsonic boundary layers, ρ_w/ρ is approximately 1.0 throughout the boundary layer and Eq. (26) can be written as

$$\frac{u}{u_\infty} \approx \left\{1 - \frac{\Delta\phi_{local}}{\Delta\phi_w}\right\}^{\frac{1}{2}} \qquad (27)$$

Velocity ratios calculated by Eqs. (26) and (27) differ by less than two percent at every point in the boundary layer for the experiments conducted in this study. The approximation given by Eq. (27) allows boundary-layer velocity profiles to be obtained from measurements of the fringe shifts appearing on the holographic interferogram without the need of knowing any other quantities about the flow. Data reduction using Eq. (27) will be referred to as Method 2.

4.2.2 Whitfield and High Relation

The velocity-temperature relationship presented by Whitfield and High (Ref. 13) and used by Whitfield (Ref. 9) and Benek (10) in reducing pitot probe data was used as an additional relation for calculating velocity ratio. The expression is the one given as Eq. (2).

The value of the velocity ratio, u/u_∞, at a point was found by calculating ρ/ρ_∞ using Eq. (21) and then using Eq. (19) to find T/T_∞.

A binary or half-interval search technique was used to determine the value of u/u_∞ that would satisfy Eq. (2) for the calculated value of T/T_∞. This method of calculation will be referred to as Method 3.

4.3 CALCULATION OF BOUNDARY-LAYER PARAMETERS

Three methods for calculating velocity from the fringe shifts appearing on holographic interferograms have been developed. All three methods were used in conjunction with the values of ρ/ρ_∞ from Eq. (21) to calculate displacement thickness, δ^*, momentum thickness, θ, shape factor, H, and skin friction, c_f. The method for performing these calculations was identical to the one described in Section 3.2. The results from the holographic interferometry data reduction were compared to probe measurements for similar flow conditions.

5.0 PRESENTATION AND DISCUSSION OF EXPERIMENTAL RESULTS

Laser holographic interferograms were made at tunnel free-stream Mach numbers of 0.50 and 0.65. The density variations obtained from the fringes on the interferograms were reduced by the three data reduction methods described in the previous section. The density and velocity profiles obtained were used to calculate the boundary-layer displacement thickness, δ^*, momentum thickness, θ, shape factor, H, and skin friction, c_f, in the manner described in Section 3.2.

A comparison of the three interferometry data reduction methods will now be presented, as well as a comparison of the interferometry results with pitot, hot-wire and split-film data.
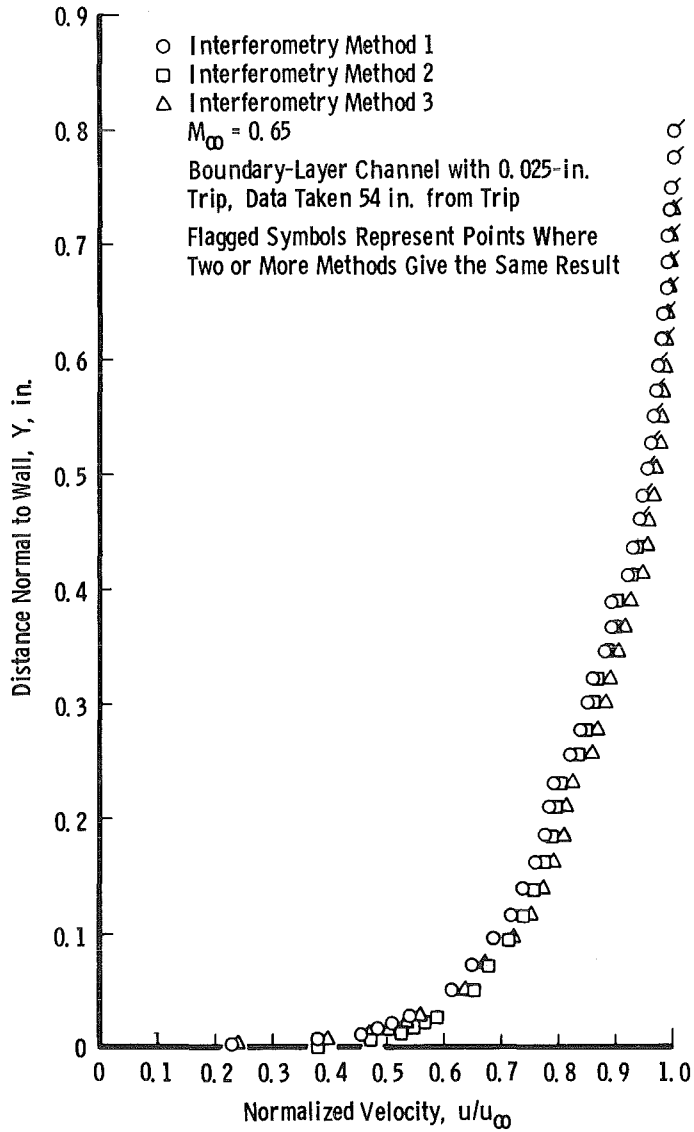
5.1 COMPARISON OF BOUNDARY-LAYER VELOCITY PROFILES

Comparisons of the boundary-layer velocity profiles calculated by the three interferometry data reduction methods are given in Fig. 13 for
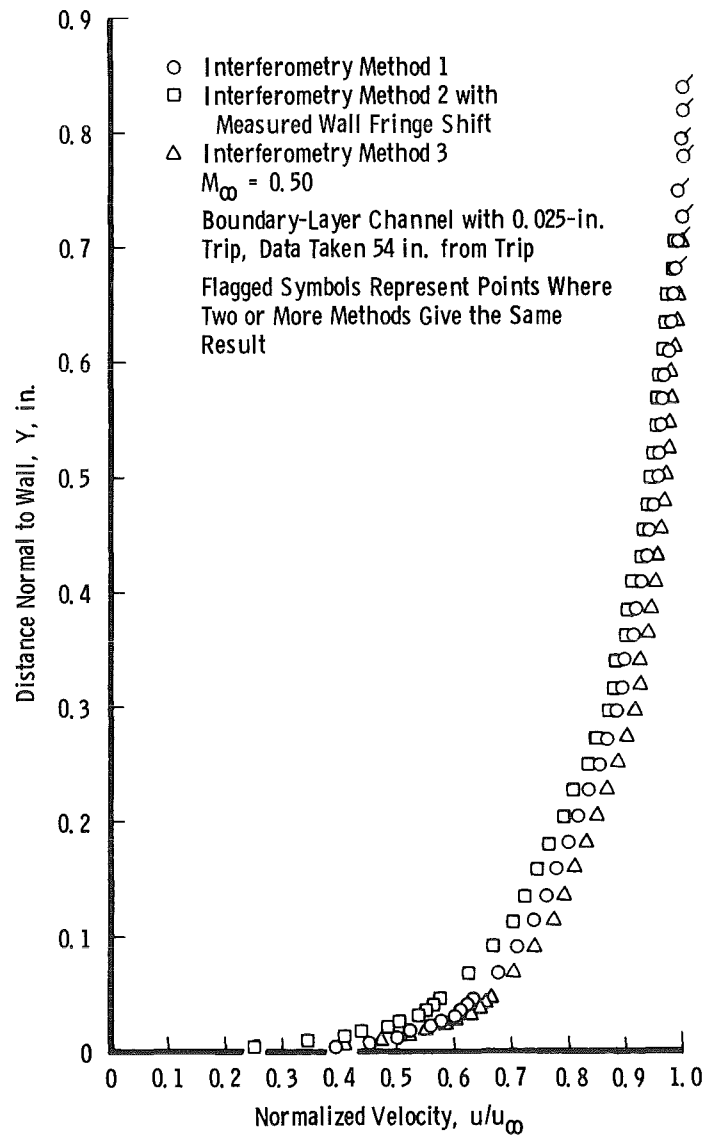
a. $M_\infty = 0.50$

Figure 13. Comparison of boundary-layer velocity profiles obtained by various holographic interferometry data reduction techniques.

b. $M_\infty = 0.65$
Figure 13. Concluded.

Mach numbers 0.50 and 0.65. As can be seen, the profiles vary slightly
from one another. Methods 1 and 3 agree quite well near the wall;
however, Method 3 produces a velocity profile that is more full than
the one resulting from Method 1. This effect is attributed to the
difference in the velocity-temperature relationship assumed for each
method. The velocities calculated by Methods 1 and 2 have a difference
which is a maximum near the wall and becomes less as the free stream is
approached. This variation is caused by errors in evaluating the fringe
shift at the wall, which is necessary for reducing the data by Method 2.
This problem arises because of the difficulty in discerning the exact
location of the intersection of the wall with the shifted fringe. If
Eq. (21) is used to calculate the fringe shift at the wall, then Methods
1 and 2 give essentially the same result.

An important consideration in any data acquisition system is repeat-
ability of results. Figure 14 presents comparisons of velocity profiles
for the three methods obtained from two independent readings of the same
interferogram. One would expect that the two independent readings from
the same interferogram would produce the same velocity profile for a
given data reduction method. All three methods show good agreement,
with Method 2 showing the best and Method 3 the worst.

In Fig. 15, velocity profiles calculated by holographic in-
terferometry Method 1 are compared with probe data for Mach numbers
0.50 and 0.65. Experience has shown that boundary-layer profiles
obtained by this method agree better with probe data than either Method
2 or 3. It was expected that Method 3 would have shown the better
agreement with probe data because this method used the same velocity-
temperature relation as was used in the probe data reduction. The cause
of the discrepancy was probably the result of neglecting the sidewall
boundary layer. Lucci (Ref. 17) found that the effect of including the
sidewall boundary layer in the data reduction equations was to remove
some of the fullness from the profile. This correction would be in the
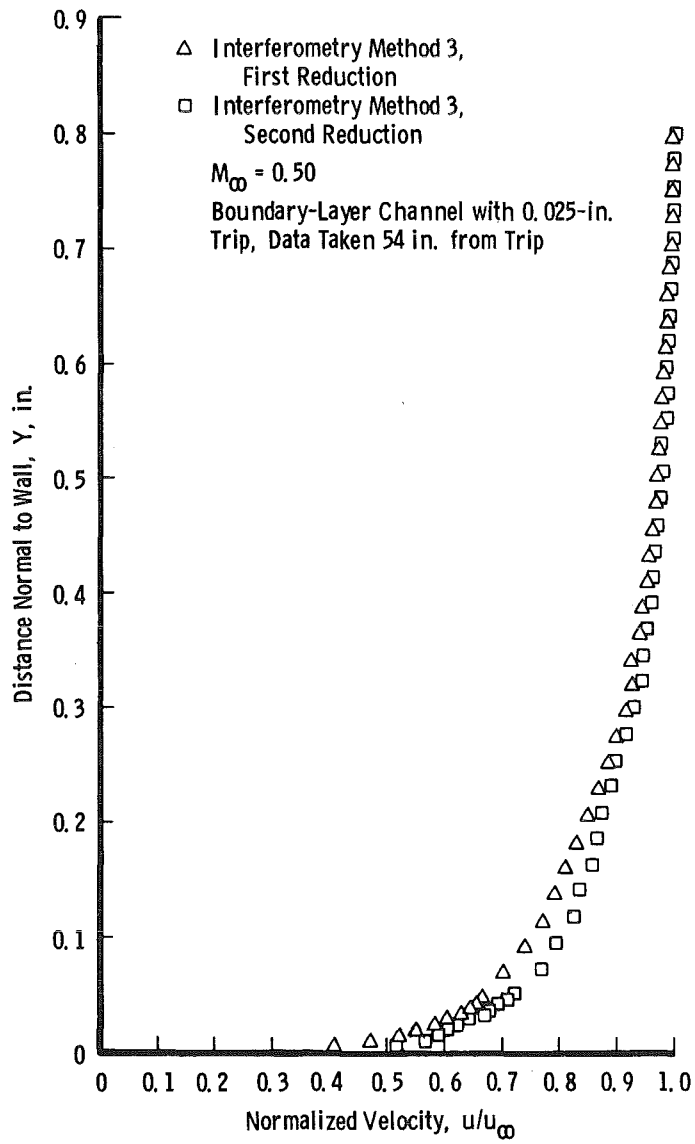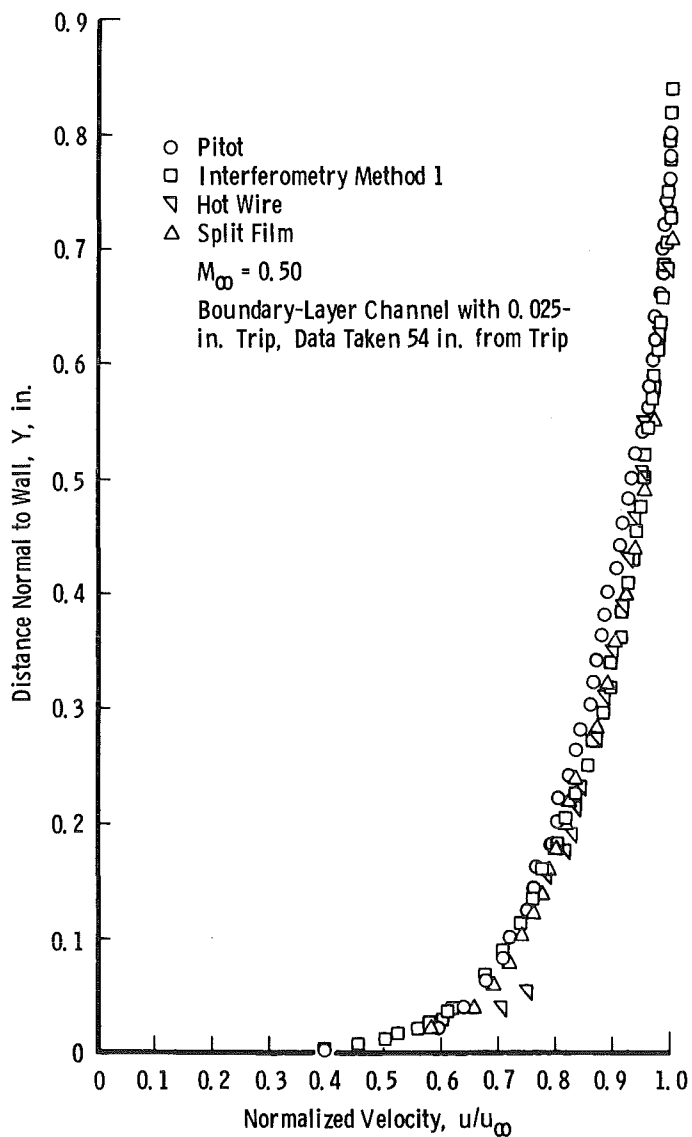proper direction to improve agreement with probe data.
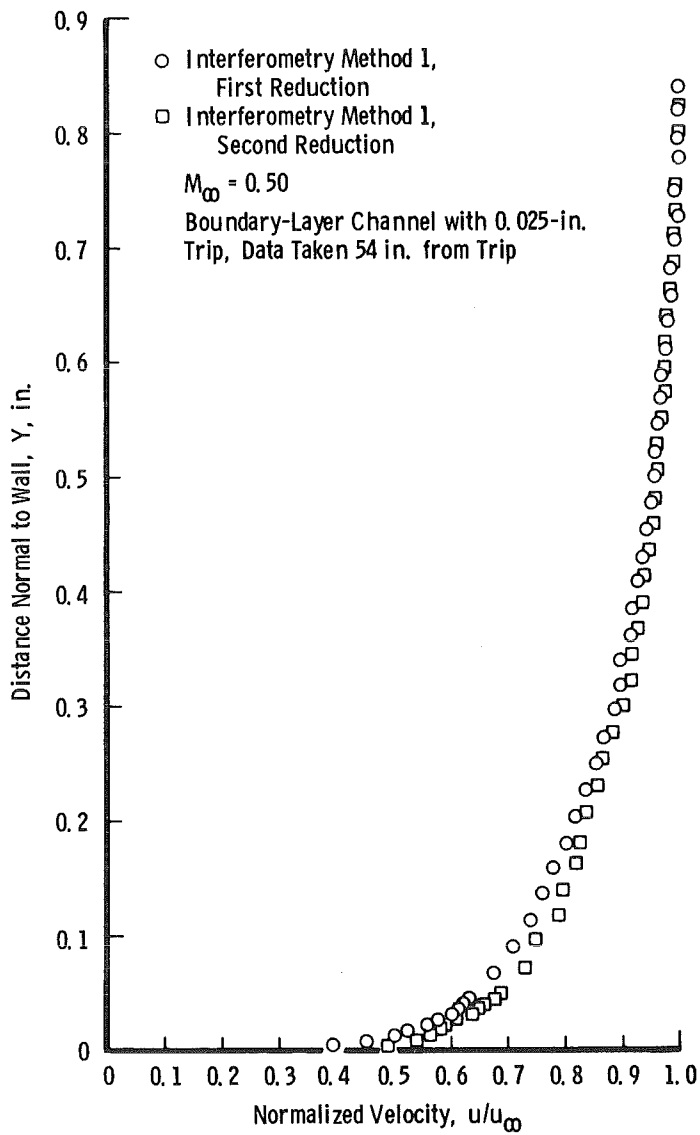
a. Method 1

Figure 14. Comparison of independently reduced interferometry data from same hologram.
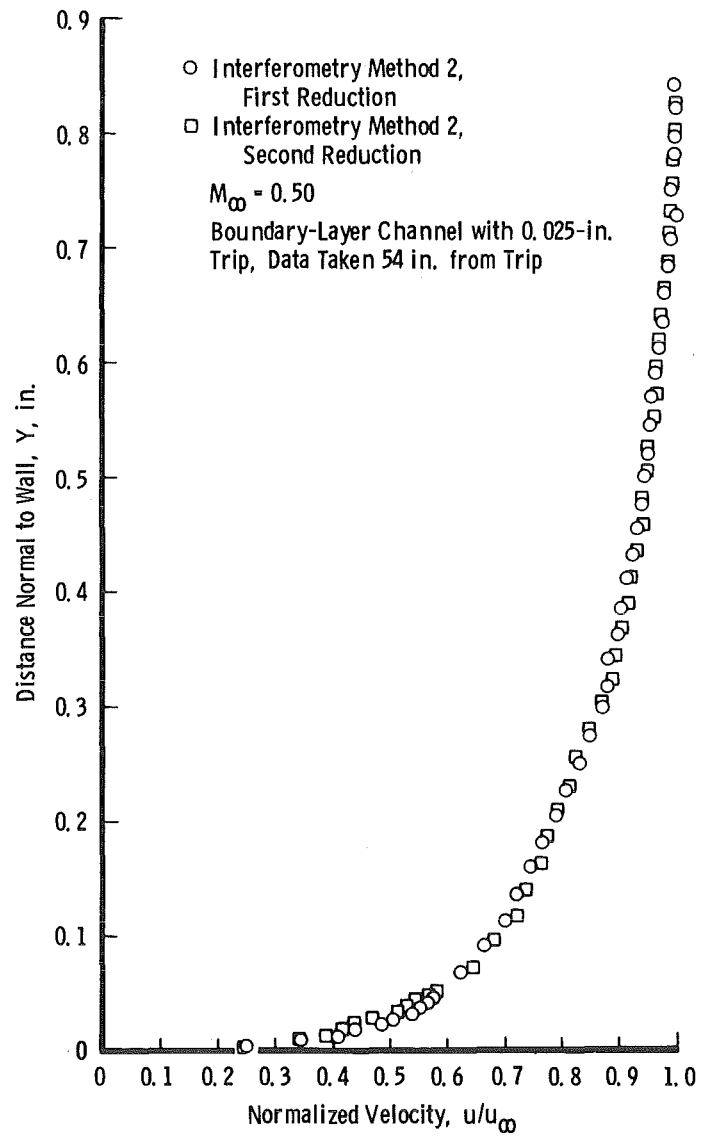
b. Method 2
Figure 14. Continued.

c. Method 3
Figure 14. Concluded.

a. $M_\infty = 0.50$

Figure 15. Comparison of velocity profiles obtained by pitot, hot-wire, split-film probes, and holographic interferometry.
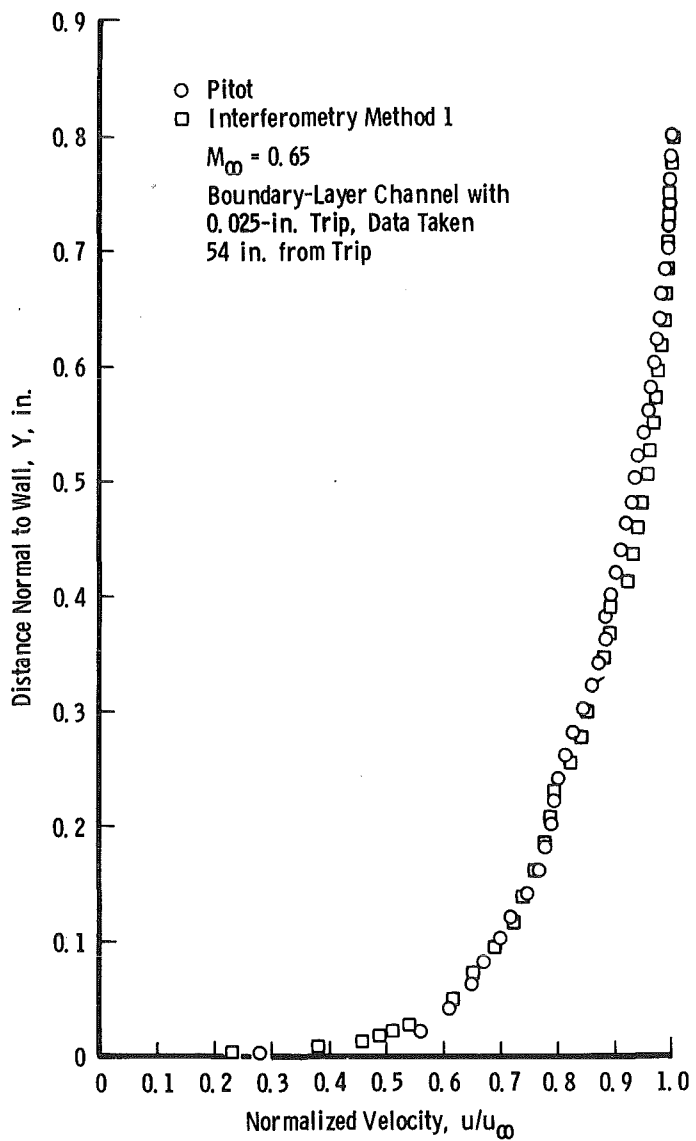
b. $M_\infty = 0.65$

Figure 15. Concluded.

5.2 COMPARISON OF BOUNDARY-LAYER PARAMETERS

The boundary-layer parameters for the velocity profiles in Figs. 13, 14, and 15 are presented in Figs. 16 and 17. In these figures, the open symbols represent pitot, hot-wire, and split-film data obtained by Benek (Ref. 10), whereas the closed symbols represent interferometry data as indicated in each figure.

In Fig. 16a, displacement thickness, δ^*, is plotted versus Reynolds number based on distance from the trip, R_x. There appears to be a considerable amount of scatter in the data; however, the trend of the probe data is also seen in the interferometry data.
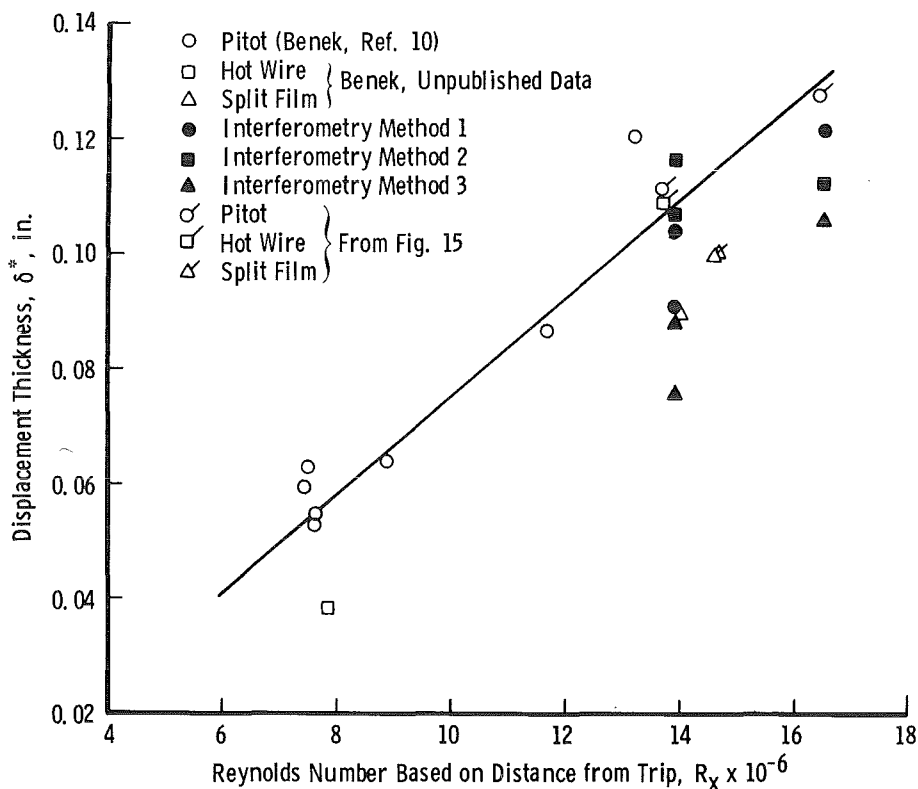
a. Displacement thickness, δ^*

Figure 16. Integrated boundary-layer properties versus Reynolds number based on distance from trip.

Momentum thickness, θ, is plotted versus Reynolds number, R_x, in Fig. 16b. The figure shows that the interferometry data have the same trend as the data obtained minus probes. Again, there is some scatter in the data.

Figure 16c is a plot of the shape factor, H, versus Reynolds number, R_x. As expected, the shape factor is only slightly dependent on Reynolds number. Again, the interferometry results show reasonable agreement with the probe data.

Figure 17 shows skin friction coefficient, c_f, plotted versus Reynolds number based on momentum thickness, R_θ. As may be seen, the skin friction decreases with increasing Reynolds number, and the interferometry results agree quite well with the probe data.
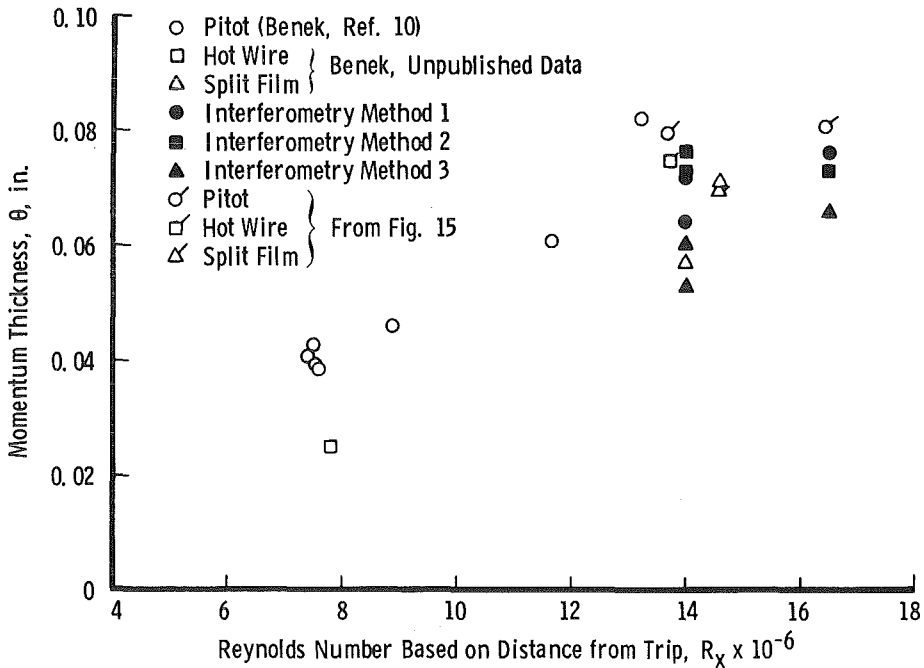
b. Momentum thickness, θ

Figure 16. Continued.
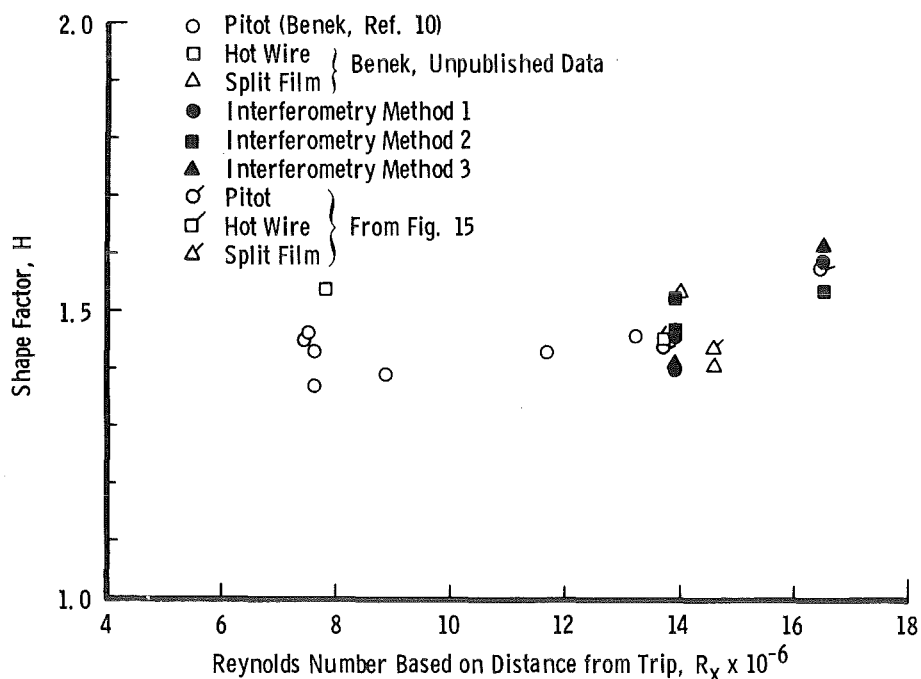
c. Shape factor, H
Figure 16. Concluded.
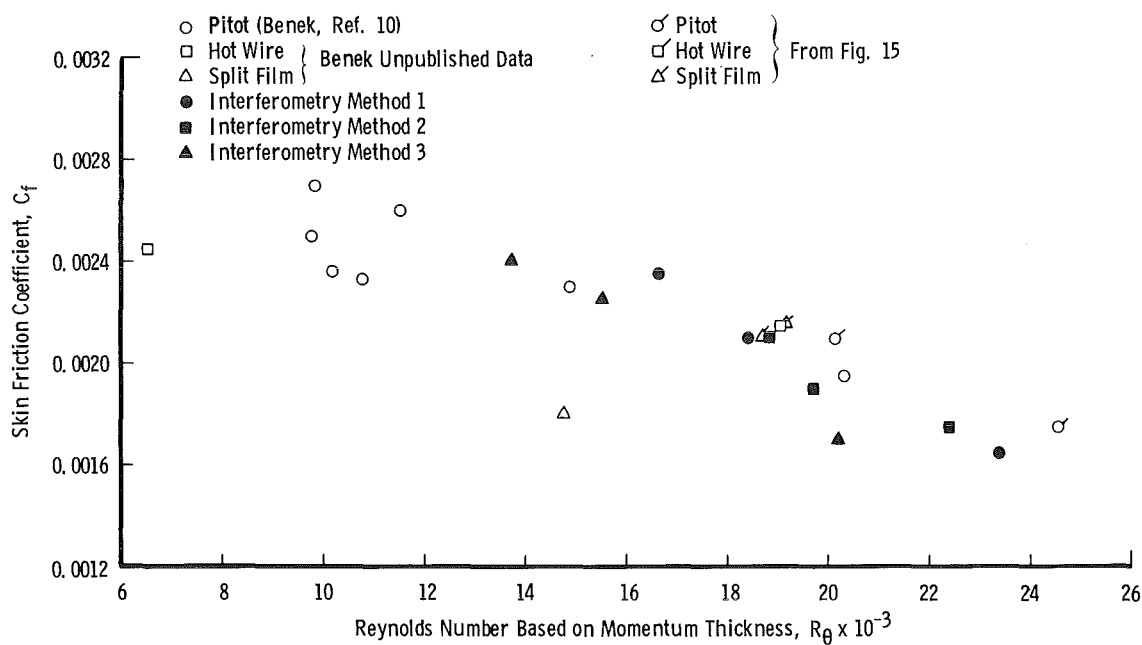
Figure 17. Skin friction coefficient versus Reynolds number based
on momentum thickness.

In general, the first interferometry data reduction method gave results that compared quite well with the pitot, hot-wire, and split-film methods. For a two-dimensional boundary layer, the interferometry technique is more appealing in that probe interference is eliminated and data acquisition time is greatly reduced. However, further work is needed to extend the data reduction technique to include holographic interferograms produced under nonadiabatic wall conditions and to account for the effect of the sidewall boundary layer.

6.0 CONCLUSIONS AND RECOMMENDATIONS

For the present application to two-dimensional subsonic flow, the finite fringe holographic interferometry technique appeared to do as good a job in performing boundary-layer measurements as the hot-wire and split-film probes. The holographic interferometry technique has the advantages of not interfering with the flow and that the data acquisition time is much less than with a probe.

Of the three data reduction equations developed, Method 1 (which uses the modified Crocco velocity-temperature relationship) appeared to give the best results. It is felt that improvements could be realized if several modifications were made to the data acquisition and reduction procedures, as follows.

First, a major problem associated with the holographic interferometry technique was the blurred image of the wall caused by the reflected light from its surface. This, coupled with the fringe intersecting the wall, made it difficult to discern the exact location of the surface. For accurate measurements of distance from the wall, Y, and the proper evaluation of the fringe shift at the wall, it is necessary to define the location of the surface correctly. This problem could be solved by placing a reference mark on the optical window at a known distance above the wall to provide a reference point uneffected by fringes and reflected light.

An improvement of the data acquisition system could be made by adapting the dual-hologram technique presented by Radley and Havener (Refs. 1 through 4). This would eliminate the difficulty of aligning the photographic-plate-translating mechanism parallel to the tunnel wall. Many holograms produced during this study proved to be worthless because of misalignment.

Finally, it is recommended that the data reduction equations be modified to include nonadiabatic wall data and to account for the effect of the sidewall boundary layer. The provision for nonadiabatic wall conditions would improve data acquisition time by eliminating the need to reach adiabatic wall conditions before data could be obtained, and the corrections for the sidewall boundary layer would increase the accuracy of the data near the wall.

REFERENCES

1. Havener, A. G. and Radley, R. J., Jr. "Turbulent Boundary Layer Flow Separation Measurements Using Holographic Interferometry." AIAA Paper No. 73-664, 6th Fluid and Plasma Dynamics Conference, Palm Springs, California, July 16-18, 1973.

2. Radley, R. J., Jr. and Havener, A. G. "The Application of Dual Hologram Interferometry to Wind Tunnel Testing." AIAA Paper No. 73-210, 11th Aerospace Sciences Meeting, Washington, D. C., January 10-12, 1973.

3. Radley, R. J., Jr. and Havener, A. G. "Dual-Hologram Interferometry: A New Technique for Wind-Tunnel Testing." Astronautics and Aeronautics, Vol. 11, No. 12, December 1973, pp. 27-29.

4. Havener, A. G. and Radley, R. J., Jr. "Supersonic Wind Tunnel Investigations Using Pulsed Laser Holography." Aerospace Research Laboratories, ARL 73-0148, October 1973.

5. Zien, T. F. and Ragsdale, W. C. "Quantitative Applications of Holographic Interferometry to Wind Tunnel Testing." Naval Ordnance Laboratory, NOLTR 74-96, December 1974.

6. Trolinger, J. D. and O'Hare, J. E. "Aerodynamic Holography." AEDC-TR-70-44 (AD709764), August 1970.

7. Kosakoski, R. A. and Collins, D. J. "Application of Holographic Interferometry to Density Field Determination in Transonic Corner Flow." AIAA Journal, Vol. 12, No. 6, June 1974, pp. 767-770.

8. Dougherty, N. S., Jr., Anderson, C. F., and Parker, R. L., Jr. "An Experimental Investigation of Techniques to Suppress Edgetones from Perforated Wind Tunnel Walls." AEDC-TR-75-88 (ADA013728), August 1975, pp. 8-11.

9. Whitfield, D. L. "Analytical, Numerical, and Experiemental Results on Turbulent Boundary Layers." AEDC-TR-76-62 (ADA027588), July 1976.

10. Benek, J. A. "Effects of Acoustic and Vortical Disturbances on the Turbulent Boundary Layer at Free-Stream Mach Number 0.5." AEDC-TR-77-73 (ADA047921), December 1977.

11. Spencer, B. W. and Jones, B. G. "Turbulent Measurements with the Split-Film Anemometer Probe." Proceedings of the Symposium on Turbulence in Liquids, University of Missouri, Rolla, 1971.

12. Sanborn, V. A. and Seegmiller, H. L. "Evaluation of Mean and Turbulent Velocity Measurements in Subsonic Accelerated Boundary Layers." NASA TM-X-62,488, March 1976.

13. Whitfield, D. L. and High, M. D. "Velocity-Temperature Relations in Turbulent Boundary Layers with Non-Unity Prandtl Numbers." AIAA Journal, Vol. 15, No. 3, March 1977, pp. 431-434.

14. Fenter, F. W. and Stalmach, C. J., Jr, "The Measurement of Local Turbulent Skin Friction at Supersonic Speeds by Means of Surface Impact Pressure Probes." Defense Research Laboratory Report DRL-392, CM-878, University of Texas, Austin, Texas, October 1957.

15. Shapiro, A. H. The Dynamics and Thermodynamics of Compressible Fluid Flow. Vol. I, New York. The Ronald Press Company, 1953, pp. 59-65.

16. Liepmann, H. W. and Roshko, A. Elements of Gas Dynamics, New York. John Wiley and Sons, Inc., 1957, pp. 153-170.

17. Lucci, C. A. "Boundary Layer Measurements in High Subsonic Flow Using Holographic Interferometry." Master's Thesis, University of Tennessee, Knoxville, Tennessee, March 1977.

APPENDIX A

PROCEDURE FOR OBTAINING FRINGE SHIFT DATA
FROM A FINITE FRINGE HOLOGRAPHIC INTERFEROGRAM

Photographs were taken of the reconstructed holograms and the portion of the negative containing the boundary layer was enlarged to improve the accuracy of the fringe shift measurements.

For this study, three methods of enlargement were used. First, the negative was placed on a photographic enlarger and a print was made of the area of interest. The second technique was to magnify the negative in a film reader designed for the purpose of making distance and angle measurements on photographs. The third method used a microfilm reader to enlarge and copy the negative. Regardless of which enlargement technique was used, the method of measuring fringe shift and distance from the wall was the same.

The method for reading fringe shifts from the negative can be explained by referring to Fig. A-1. When the photographic plate is moved parallel to the wall, a line drawn tangent to the fringes in the free-stream will be perpendicular to the wall. Therefore, a reference line was established perpendicular to the wall as shown in Fig. A-1. All fringe shift measurements were made relative to this line, and the distance, Y, above the wall was measured along the line.

Starting at the wall, the distance was measured from the reference line to the center of the fringe of interest. This was repeated at increasing values of Y until the free stream was reached (i.e., until the distance from the reference line to the fringe does not change by a measurable amount, this distance is $\Delta\phi_{ref}$). Then, $\Delta\phi_{ref}$ was subtracted from the data to give the fringe shift, $\Delta\phi$, as a function of Y.

Y - Distance above Wall
ø - Fringe Spacing
Δø - Fringe Shift
Δø_ref - Distance from Reference Line
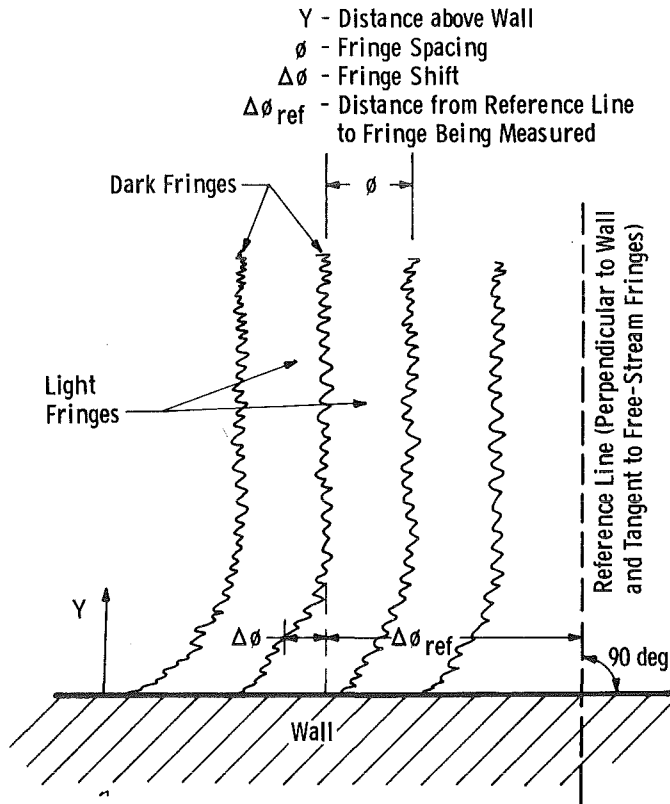to Fringe Being Measured

Figure A-1. Definition of fringe parameters.

The units in which $\Delta\phi$ was measured were unimportant as long as they were consistent with the ones used to measure the fringe width, ϕ. The fringe width is defined as the distance between the centers of two adjacent fringes of the same type and was measured as shown in Fig. A-1.

The magnification factor was removed from the measurement of Y by means of a scaling constant derived from measurement of a known reference distance appearing on the negative.

In addition to the fringe shift information, measurement of the tunnel total conditions and free-stream Mach number were necessary to complete the conversion from fringe shift to velocity profile.

NOMENCLATURE

c	Speed of light in a vacuum
c_f	Local skin friction coefficient
C_p	Constant pressure specific heat
H	Shape factor (see Eq. (5))
K	Used herein as 10m (m = 7)
k	Molecular thermal conductivity
k_t	Eddy thermal conductivity
L	Width of test section (= 6 in.)
M_∞	Free-stream Mach number
m	Defined as m = 7
n	Index of refraction (= c/ν)
Pr_m	Mixed Prandtl number (= $C_p(\mu + \mu_t)/(k+k_t)$)
P_T	Total pressure
R_x	Reynolds number based on distance from trip
R_θ	Reynolds number based on momentum thickness
$Re_{\infty,y}$	Reynolds number based on distance above wall

r   Recovery factor (= 0.88)

S   Constant sensitivity factor (= $\lambda \rho_s / L \beta \rho_\infty$)

S'   Variable sensitivity factor (= $\lambda \rho_s / L \beta \rho$)

T   Absolute temperature

T_T Total temperature

t   Time, sec

Δt Small interval of time, sec

u   Velocity

Δx Change in optical path length

Y   Distance from wall to a point in the boundary layer, in.

α Used herein as 2.5m (m = 7)

β Optical constant for a particular gas (= 0.000292 for air)

γ Ratio of specific heats (= 1.4 for air)

δ^* Displacement thickness $\left(= \int_0^{Y_\infty} \left(1 - \frac{\rho u}{\rho_\infty u_\infty} \right) dy \right)$, in.

θ Momentum thickness $\left(= \int_0^{Y_\infty} \frac{\rho u}{\rho_\infty u_\infty} \left(1 - \frac{u}{u_\infty} \right) dy \right)$, in.

ϕ Fringe spacing

$\Delta \phi$ Total fringe shift

$\Delta\phi_\infty$ Fringe shift of free stream relative to total conditions

$\Delta\phi_{local}$ Fringe shift at a point relative to the free stream

$\Delta\phi_{plenum}$ Fringe shift relative to free stream caused by density change in plenum

λ Wavelength of laser light (= 6,943 $\overset{\circ}{\text{A}}$)

ρ Local gas density

ρ_∞ Free-stream gas density

ρ_o Gas density in test section without flow

ρ_s Reference gas density at standard conditions (= 0.0807 lbm/ft^3)

μ Molecular viscosity

μ_t Eddy viscosity

ν Speed of light in a medium

SUBSCRIPTS

1   No flow

2   Flow

w   Wall value

aw   Adiabatic wall value

∞   Free-stream value